

NucleiMix: Realistic Data Augmentation for Nuclei Instance Segmentation

Jiamu Wang^a, Jin Tae Kwak^{a,*}

^a*School of Electrical Engineering, Korea University, Seoul 02841, Republic of Korea*

Abstract

Nuclei instance segmentation is an essential task in pathology image analysis, serving as the foundation for many downstream applications. The release of several public datasets has significantly advanced research in this area, yet many existing methods struggle with data imbalance issues. To address this challenge, this study introduces a data augmentation method, called as NucleiMix, that is designed to balance the distribution of nuclei types by increasing the number of rare-type nuclei within datasets. NucleiMix operates in two phases. In the first phase, it identifies candidate locations similar to the surroundings of rare-type nuclei and inserts rare-type nuclei into the candidate locations. In the second phase, it employs a progressive inpainting strategy using a pre-trained diffusion model to seamlessly integrate rare-type nuclei into their new environments in replacement of major-type nuclei or background locations. We systematically evaluate the effectiveness of NucleiMix on three public datasets using two popular nuclei instance segmentation models. The results demonstrate the superior ability of NucleiMix to synthesize realistic rare-type nuclei and to enhance the quality of nuclei segmentation and classification in an accurate and robust manner.

Keywords: Data Augmentation, Diffusion Model, Nuclei Instance Segmentation, Pathology

1. Introduction

In recent years, the combination of large-scale pathology data and advanced artificial intelligence techniques has fueled the development and ad-

*Corresponding author: Tel.: +0-000-000-0000; fax: +0-000-000-0000;

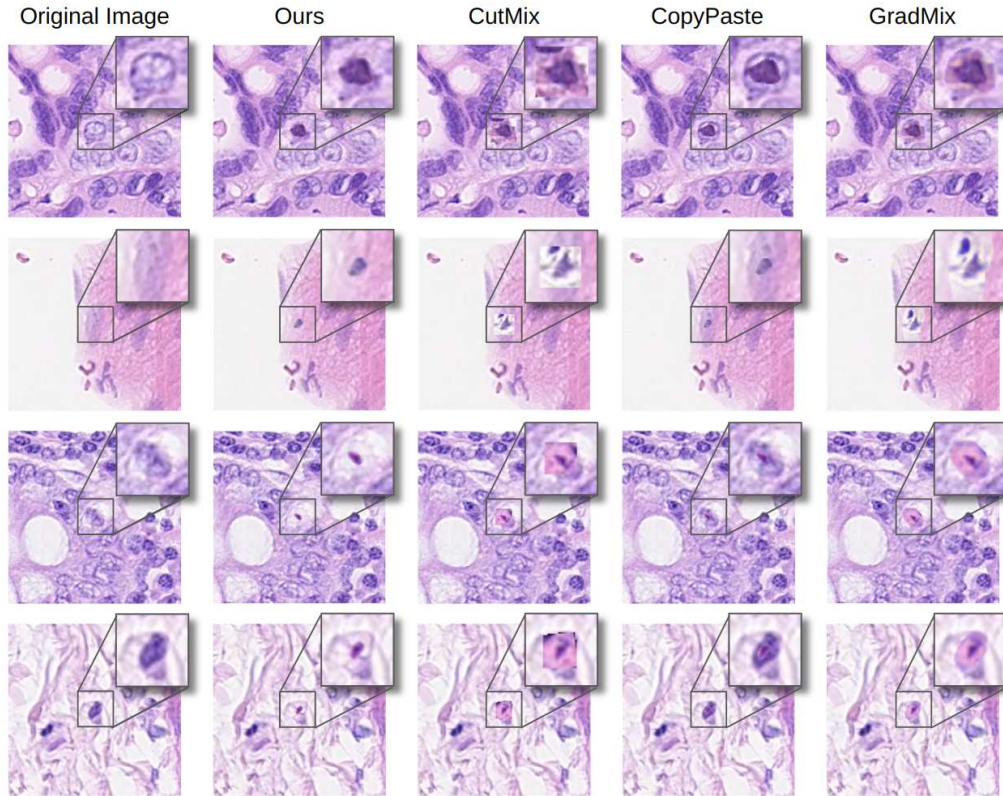


Figure 1: Comparison of nuclei augmentation between NucleiMix with other augmentation methods.

vancement of numerous digital pathology tools. These include cancer detection and grading He et al. (2012), tissue sub-typing Barocas et al. (2007), nuclei segmentation and classification Graham et al. (2019), and survival prediction Burke et al. (1997). Among these, nuclei instance segmentation has gained much attention due to its critical role in pathology image analysis, as the count, shape, and distribution of nuclei are tightly related to the nature of diseases and cellular microenvironments Kumar et al. (2017a). Nuclei instance segmentation involves identifying and delineating individual cell nuclei within pathology images. Deep learning models have substantially improved the accuracy of nuclei instance segmentation Graham et al. (2019); Doan et al. (2022b), but they generally require a large amount of

labeled datasets. Unfortunately, acquiring these labels is both costly and time-consuming, presenting a significant challenge. Despite such challenges, there arise several public datasets, containing extensive annotations with differing types of cells and nuclei, such as ConSeP Graham et al. (2019), MoNuSAC Verma et al. (2021), GLySAC Doan et al. (2022b), and Pan-Nuke Gamper et al. (2019). These datasets have formed the basis for the development and validation of various nuclei segmentation and classification models Hollandi et al. (2022). However, the types of cells/nuclei and their distributions substantially vary, i.e., such a dataset, in general, is greatly imbalanced. This imbalance, particularly the under-representation of rare cells/nuclei types, substantially contributes to the performance degradation of the deep learning models Nunes et al. (2024). Data augmentation techniques have proved efficient and effective in addressing the shortcomings of existing data and annotations by enlarging the dataset size and enriching data diversity. Earlier methods including random flipping, rotating, and cropping are popular and have been successfully applied to numerous applications [Takahashi et al. (2019), Hussain et al. (2017), Sirazitdinov et al. (2019), Feng et al. (2020)]. Later, more sophisticated mix-based data augmentation techniques, such as MixUp (Zhang et al., 2017), CutOut (DeVries et al., 2017), CutMix (Yun et al., 2019), CopyPaste Ghiasi et al. (2021), and GradMix (Doan et al., 2022a), have been proposed to further enhance the performance of deep learning models. These existing mix-based data augmentation methods often overlook the effect of augmentation on neighboring regions, leading to unnecessary artifacts, particularly in nuclei data (Fig. 1). For example, CutMix crops a whole bounding box including an object, e.g., a nucleus, and pastes it into a random location, resulting in an obvious rectangular artifact. CopyPaste crops only the object and paste it randomly. GradMix proposes to conduct a weighted sum between the cropped region and the background region but still leaves an unnatural transition zone around the object. To address the mentioned challenges, we propose NucleiMix, a method designed to create realistic augmented images with various instances of nuclei. NucleiMix aims to balance and enrich nuclei data, thereby leading to improved nuclei instance segmentation. NucleiMix adopts a copy-paste approach to increase the number of under-represented instances of nuclei by using the existing instances. In other words, it copies an under-represented nucleus from the dataset and pastes it into a target location. However, a simple copy-paste approach can introduce the following issues: 1) Random location: it randomly chooses the target regions that

may severely differ from the original environment of the selected nuclei; 2) Artifacts: it often creates unrealistic and unnecessary artifacts around the pasted nuclei; 3) Obscure boundary: it often loses the clarity of the nuclei boundary. To tackle these issues, NucleiMix introduces two strategies: 1) Context-aware probabilistic sampling and 2) Progressive inpainting using a diffusion model (Song et al., 2020b; Sohl-Dickstein et al., 2015; Ho et al., 2020; Chung et al., 2022b). Context-aware probabilistic sampling employs an unsupervised Gaussian Mixture Model (GMM) (Reynolds and A., 2009) to learn the distribution of nuclei along with their surrounding regions and sample target nuclei with environments resembling those of under-represented nuclei. For each target region, it samples the most likely nucleus from the pool of under-represented nuclei. Progressive inpainting with a diffusion model generates realistic backgrounds for the under-represented nuclei in two steps, ensuring seamless integration with the existing environment of the target region. In the first step, it removes the nucleus in the target region and then inpaints it to create a smooth, clean background. In the second step, it places the under-represented nucleus along with its immediate one-layer contour (preserving its immediate background information) and removes its second and third contours, establishing a transitional zone. This transitional zone is inpainted to smoothly blend the nucleus with the surrounding area.

To prove the effectiveness of our method, we conduct extensive experiments on three public datasets, including CoNSeP (Graham et al., 2019), GLySAC (Doan et al., 2022b), and MoNuSAC (Verma et al., 2021). The experimental results show that NucleiMix is able to generate realistic, augmented images for nuclei data and mitigate the challenges posed by data imbalance, leading to improved nuclei instance segmentation.

2. Related Works

Enhancing dataset size and diversity significantly improves the robustness of deep learning models and helps mitigate overfitting. However, collecting medical image datasets is notably challenging and costly due to the exhaustive annotation required and concerns about patient privacy. In response to these challenges, data augmentation has emerged as an efficient solution to address the scarcity of data by effectively increasing dataset heterogeneity. NucleiMix, our novel mix-based data augmentation technique, is tailored specifically for histopathology datasets with accurate pixel-wise annotations.

This section discusses traditional data augmentation methods alongside several innovative mix-based techniques.

2.1. Traditional Data Augmentation

Traditional data augmentation methods primarily focus on spatial and color transformations to diversify image presentations Cossio and M. (2023). Several spatial transformations have been widely adopted for various applications. For instance, random cropping randomly chooses a rectangular area within an image and uses it as a new image, helping the model extract features with different scales of views; random rotation randomly rotates an image by an angle within a specific range; vertical and horizontal flip apply vertical or horizontal mirroring to an image. Adjusting color and contrast is also a popular technique for data augmentation, which modifies the color tone or intensity levels of an image. For example, brightness adjustment alters the intensity values of an image, making it either darker or brighter compared to the original brightness; contrast adjustment applies a linear transformation to the intensity range Tellez et al. (2019) of an image; saturation modifies color intensity by multiplying a random color channel with a scalar factor Naglah et al. (2022); hue adjustment randomly shifts color channels. Furthermore, there are other popular methods such as noise-based methods, adding Gaussian or Poisson noise on an image, and blur/unsharp-based methods, blurring images with Gaussian or median filters.

2.2. Mix-based Data Augmentation

Mix-based data augmentation methods typically combine two or more images and blend them together to create a composite image. MixUp Zhang et al. (2017) combines two random images by blending them in the alpha channel and generates a new label by taking a linear combination of the two original labels. CutOut DeVries et al. (2017) randomly masks a rectangular portion of an image, simulating dropout effects on input to deep learning models. Similar to CutOut, CutMix Yun et al. (2019) also masks a random portion of an image, but it fills the masked area with a portion taken from another image, simulating an occlusion in an image and increasing the diversity of image data. While these methods are generic and applicable to various tasks, there have also been specific efforts to develop tailored data augmentation methods for nuclei segmentation in pathology images. For instance, GradMix Doan et al. (2022a) finds pairs of major-type nuclei and rare-type (under-represented) nuclei that meet specific shape constraints and replace

the larger major nuclei with the relatively smaller rare-type nuclei. To alleviate the differences in the surrounding environments, GradMix linearly blends the neighboring region of the major-type nuclei with that of rare-type nuclei. Though it has shown to be effective in improving nuclei segmentation and classification, it has been only evaluated on a single nuclei dataset.

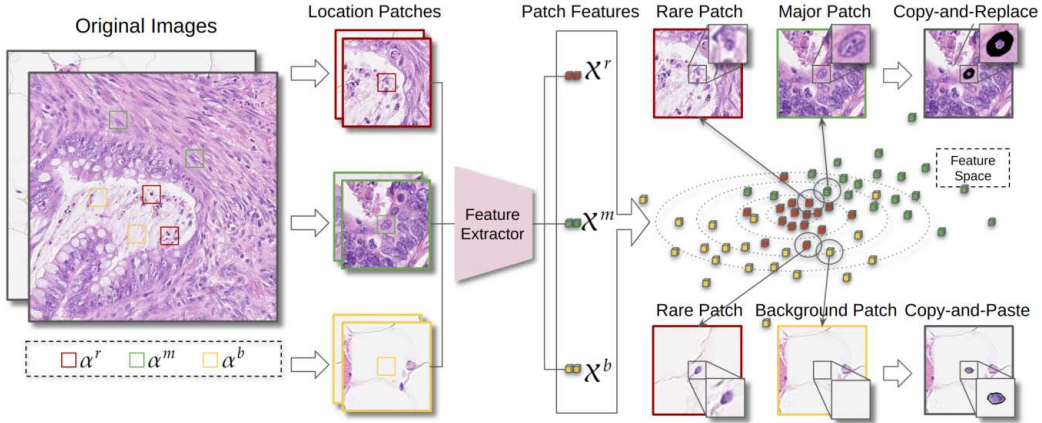


Figure 2: The procedure of context-aware probabilistic sampling for the selection of candidate locations. First, we collect all rare-type (α^r in red), major-type (α^m in green), and background (α^b in yellow) locations from the training dataset. Second, we crop the location patches for all the locations and feed them into a pre-trained feature extractor to extract the corresponding feature vectors (rare-type feature \mathcal{X}^r in red, major-type \mathcal{X}^m in green, and background \mathcal{X}^b in yellow). Third, we sample a major-type feature vector (green cube) or background feature vector (yellow cube) that is close to the rare-type feature vector distribution (red cubes) and get the most suitable major-type or background location. Finally, we sample an instance of rare-type nuclei that is closest to the target major-type location in the feature space and copy the rare-type nucleus to replace the major-type nucleus (Copy-and-Replace on the right-top). Similarly, for the target background location, we copy the rare-type nucleus and paste it onto the background location (Copy-and-Paste on the right-bottom).

3. Methodology

Suppose that we are given a dataset of pathology images \mathcal{D} containing a number of nuclei $\{\alpha_i | i = 1, \dots, N\}$ where α_i is the i th nucleus. Each α_i is assigned a distinct class label $y_i \in \{1, \dots, C\}$ where C is the cardinality of nuclear types. Among C nuclear types, at least one type is under-represented

in \mathcal{D} , identified as rare-type nuclei $\mathcal{A}^r = \{\alpha_i^r | i = 1, \dots, N_r\}$, and the remaining types are regarded as major-type nuclei $\mathcal{A}^m = \{\alpha_i^m | i = 1, \dots, N_m\}$ where N_r and N_m denote the number of rare-type and major-type nuclei, respectively, and there are $N = N_r + N_m$ and $N_r \ll N_m$. In addition, certain locations \mathcal{D} are collected and referred to as background locations $\mathcal{A}^b = \{\alpha_i^b | i = 1, \dots, N_b\}$ where N_b is the number of background locations. These locations contain neither major-type nor rare-type nuclei. Given these three types of locations, NucleiMix strategically positions existing rare-type nuclei into locations where major-type nuclei are present or no nuclei are present (background locations), but where the neighboring environments are similar to those of rare-type nuclei. Then, it blends the original environment (of either major-type nuclei or background locations) with the inserted rare-type nuclei in a way that preserves the texture of the original environment as well as the shape and sharpness of the rare-type nuclei. The detailed procedures are outlined in the Algorithm 1.

3.1. Context-aware Probabilistic Sampling: Candidate Locations

We consider three distinct types of locations: rare-type, major-type, and background locations. These are characterized by the presence and type of nuclei in the corresponding locations. To analyze the neighboring environment of these locations, we first crop an image patch of size 224×224 pixels around each identified location. Subsequently, we remove the central portion of size 112×112 pixels for rare-type and major-type nuclei and fill the void region using a Navier-Stokes-based inpainting method Ebrahimi et al. (2013). Formally, we define rare-type patches as $\mathcal{P}^r = \{\phi_i^r | i = 1, \dots, N_r\}$, major-type patches as $\mathcal{P}^m = \{\phi_i^m | i = 1, \dots, N_m\}$, and background patches as $\mathcal{P}^b = \{\phi_i^b | i = 1, \dots, N_b\}$. Here, ϕ_i^r , ϕ_i^m , and ϕ_i^b represent the patches centered around α_i^r , α_i^m , and α_i^b , respectively.

Each patch ϕ_i^r , ϕ_i^m , and ϕ_i^b is fed into a feature extractor to generate feature vectors $x_i^r, x_i^m, x_i^b \in \mathbb{R}^p$ where p is 16. This process results in three sets of feature vectors: rare-type feature vectors $\mathcal{X}^r = \{x_i^r \in \mathbb{R}^p, i = 1, \dots, N_r\}$, major-type feature vectors $\mathcal{X}^m = \{x_i^m \in \mathbb{R}^p, i = 1, \dots, N_m\}$, and background feature vectors $\mathcal{X}^b = \{x_i^b \in \mathbb{R}^p, i = 1, \dots, N_b\}$. We use a pre-trained CTransPath Wang et al. (2022) as a feature extractor. Provided with \mathcal{X}^r , we utilize a GMM to learn the distribution of the environment surrounding rare-type nuclei, modeled as $p(\mathcal{P}^r) = p(\mathcal{X}^r) = \mathcal{N}(\mu^r, \Sigma^r)$ where μ^r and Σ^r denote the mean and covariance matrix of the rare-type feature vectors \mathcal{X}^r , respectively. This model is then used to predict the likelihood

of the major-type and background feature vectors by measuring how closely they resemble rare-type feature vectors. These likelihood are expressed as $p(\mathcal{P}^m | \mathcal{P}^r) = \mathcal{N}(\mathcal{X}^m | \mu^r, \Sigma^r)$ and $p(\mathcal{P}^b | \mathcal{P}^r) = \mathcal{N}(\mathcal{X}^b | \mu^r, \Sigma^r)$, respectively. In other words, we conjecture that the neighboring environment of α_i^m or α_i^b is similar to that of rare-type nuclei if $p(\phi_i^m | \mathcal{P}^r)$ or $p(\phi_i^b | \mathcal{P}^r)$ is high.

Next, we sample candidate locations to insert rare-type nuclei from major-type and background patches based on the joint likelihood $\hat{\phi}^t \sim p(\mathcal{P}^m, \mathcal{P}^b | \mathcal{P}^r)$, where t is either m or b . Here, $\hat{\phi}^t$ are the patches that share similar neighboring environments with the rare-type patches \mathcal{P}^r . For each $\hat{\phi}^t$, we choose a specific rare-type nucleus that best matches the new neighboring environments based upon the probability distributions given by:

$$p(\phi_i^r | \hat{\phi}^t) = \frac{e^{-w_i \times D(\hat{\phi}^t, \phi_i^r)}}{\sum_{k=1}^{N_r} e^{-w_k \times D(\hat{\phi}^t, \phi_k^r)}} \quad (1)$$

where w_i is a weight associated with α_i^r , $D(\hat{\phi}^t, \phi_i^r) = \|\hat{x}^t - x_i^r\|_2$, \hat{x}^t is the feature vectors of $\hat{\phi}^t$, and $\|\cdot\|_2$ denotes the L2 distance. Sampling the most likely rare-type patches for the major-type and background locations, designated as $\phi^{r|m}$ and $\phi^{r|b}$, we insert the corresponding rare-type nuclei into these selected locations, respectively.

For the major-type location, we remove the existing major-type nucleus and replace it with a new rare-type nucleus. This process can be understood as a Copy-and-Replace operation. As for the background location, we directly insert a new rare-type nucleus, which can be described as a Copy-and-Paste operation. The entire procedure is illustrated in Fig. 2.

3.2. Progressive Inpainting with Diffusion Model

Although the above approach effectively identifies the patches with similar neighboring environments, the simple placement of rare-type nuclei can still result in artifacts or discontinuities surrounding the inserted nuclei. Generative models such as GAN Goodfellow et al. (2022) or diffusion models Sohl-Dickstein et al. (2015); Ho et al. (2020) can be adopted to fill in the artificial, discontinuous, or missing regions. However, we have observed that such direct inpainting can sometimes lead to blurry or obscure boundaries around the inserted nuclei. As shown in Fig.3, existing diffusion models tend to harmonize the inpainted regions with their surroundings, which can result in a loss of sharpness at the nuclear boundaries. To address such issues, we introduce a progressive inpainting strategy that can preserve the integrity of

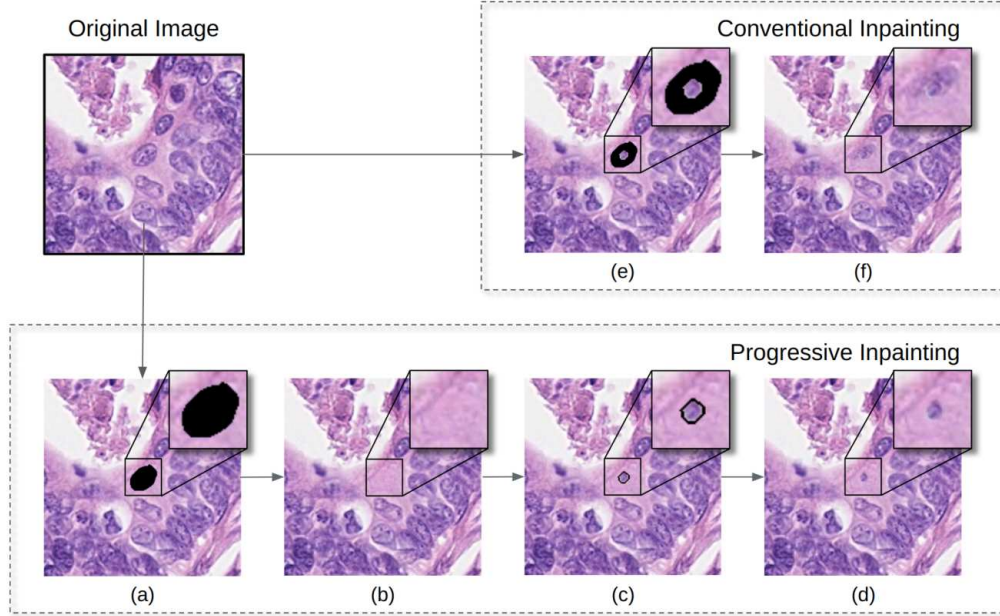


Figure 3: The procedure of the progressive inpainting strategy. Selecting a major-type location, the progressive inpainting strategy (a) removes the major-type nucleus, (b) inpaints the blank region using a diffusion model, (c) places a rare-type nucleus with an immediate one-layer contour from the original environment and two-layers of a transition zone, and (d) inpaints the transition zone using the diffusion model. In contrast, the conventional method (e) places the rare-type nucleus in the blank region and (f) applies inpainting directly to the blank region.

the inserted nuclei while seamlessly integrating them into the surrounding environments. The proposed method conducts inpainting in two stages with distinct constraints applied to the diffusion model. In the first stage, for a major-type location $\hat{\phi}^m$, we erase the region previously occupied by a major-type nucleus $\hat{\alpha}^m$, creating a blank space, and use a diffusion model to inpaint this blank region. For a background location $\hat{\phi}^b$, we skip the first stage and proceed to the second stage. In the second stage, we position rare-type nuclei, $\alpha^{r|m}$ and $\alpha^{r|b}$, at the center of the major-type and background patches, $\hat{\phi}^m$ and $\hat{\phi}^b$, respectively. To preserve the original neighborhood information, the immediate one-layer contour surrounding $\alpha^{r|m}$ and $\alpha^{r|b}$ is placed together. We then create a transition zone around the inserted rare-type nuclei by removing the second and third-layer contours surrounding them. The diffu-

sion model is utilized once again to inpaint the transition zone, achieving a seamless transition with the surrounding environments.

3.3. Diffusion Model: Solving Inverse Problems

Diffusion models define the forward diffusion process as a Markov Chain where the data is gradually corrupted by adding noise, while their generative process reverses this noising process to recover the original data. Song et al. (2020b) defines both forward and generative processes as *Itô* stochastic differential equations (SDEs). Let $\mathbf{x}_t \in \mathbb{R}^d, \forall t \in [0, T]$ be a continuous diffusion process such that $\mathbf{x}_0 \sim p_{data}$ is data distribution and $\mathbf{x}_T \sim p_T$ is isotropic Gaussian distribution. The forward SDE is given in the form of:

$$d\mathbf{x} = -\frac{\beta(t)}{2}\mathbf{x}dt + \sqrt{\beta(t)}d\mathbf{w} \quad (2)$$

where $\beta(t)$ is bounded positive noise schedule series and \mathbf{w} is the standard Brownian motion. The coupled reverse SDE of (2) can be written down as Anderson and DO. (1982):

$$d\mathbf{x} = \left[-\frac{\beta(t)}{2}\mathbf{x} - \beta(t)\nabla_{\mathbf{x}_t} \log p_t(\mathbf{x}_t) \right] dt + \sqrt{\beta(t)} d\bar{\mathbf{w}} \quad (3)$$

where dt is an infinitesimal negative time step and $d\bar{\mathbf{w}}$ is the standard Brownian motion running backward in time. One can train a neural network $s_\theta(\mathbf{x}_t, t)$ to approximate the score function $\nabla_{\mathbf{x}_t} \log p_t(\mathbf{x}_t)$ by score matching, and in practice, the score function is replaced by $\nabla_x \log p_{0t}(\mathbf{x}_t|\mathbf{x}_0)$ and trained with the following denoising score matching objective:

$$\min_{\theta} \mathbb{E}_{\mathbf{x}_0 \sim p_{data}(\mathbf{x}), \mathbf{x}_t \sim p_{0t}(\mathbf{x}_t|\mathbf{x}_0)} \left[\|s_\theta(\mathbf{x}_t, t) - \nabla_{\mathbf{x}_t} \log p_{0t}(\mathbf{x}_t|\mathbf{x}_0)\|_2^2 \right] \quad (4)$$

where $t \sim U(0, T)$ and U is the uniform distribution.

The role of a diffusion model in our study is to fill the missing region in an image \mathbf{x}_0 with a masked image as the measurement \mathbf{y} , which can be formulated as an inpainting problem. We denote unknown pixels as $(\mathcal{I} - \mathcal{H}^T \mathcal{H})\mathbf{x}_0$ and measurement as $\mathbf{y} = \mathcal{H}\mathbf{x}_0$, where $\mathbf{x}_0 \in \mathbb{R}^d, \mathbf{y} \in \mathbb{R}^n, \mathcal{H} \in \{0, 1\}^{n \times d}$ Lugmayr et al. (2022); Chung et al. (2022b). Inpainting is an inverse problem to recover the data from a tractable distribution $p_t(\mathbf{y}|\mathbf{x}_t)$. Using Bayes' rule, we have the relationship: $p(\mathbf{x}|\mathbf{y}) = p(\mathbf{y}|\mathbf{x})p(\mathbf{x})/p(\mathbf{y})$, where we can utilize

$p(\mathbf{x})$ as the prior and sample from the posterior $p(\mathbf{x}|\mathbf{y})$. The score function for $p(\mathbf{x}|\mathbf{y})$ at time t is given by:

$$\nabla_{\mathbf{x}_t} \log p(\mathbf{x}_t|\mathbf{y}) = \nabla_{\mathbf{x}_t} \log p(\mathbf{x}_t) + \nabla_{\mathbf{x}_t} \log p(\mathbf{y}|\mathbf{x}_t). \quad (5)$$

We can modify (3) by replacing $\nabla_{\mathbf{x}_t} \log p(\mathbf{x}_t)$ with $\nabla_{\mathbf{x}_t} \log p(\mathbf{x}_t|\mathbf{y})$ and derive the reverse diffusion sampler for the inverse problem:

$$d\mathbf{x} = \left[-\frac{\beta(t)}{2} \mathbf{x} - \beta(t) (\nabla_{\mathbf{x}_t} \log p_t(\mathbf{x}_t) + \nabla_{\mathbf{x}_t} \log p_t(\mathbf{y}|\mathbf{x}_t)) \right] dt + \sqrt{\beta(t)} d\bar{\mathbf{w}}. \quad (6)$$

In (5), $\nabla_{\mathbf{x}_t} \log p_t(\mathbf{x}_t)$ can be approximated by a pre-trained score function $s_{\theta^*}(\mathbf{x}_t, t)$, while the latter term $\nabla_{\mathbf{x}_t} \log p_t(\mathbf{y}|\mathbf{x}_t)$ is intractable, since \mathbf{y} is only tractable from \mathbf{x}_0 as $\mathbf{y} = \mathcal{H}\mathbf{x}_0$. To be able to sample from a tractable distribution and boost the prediction performance, in our experiment, we adopt the manifold constrained gradient (MCG) Chung et al. (2022b) method. We adopt Variance Preserving SDE (VP-SDE or DDPM Ho et al. (2020)) to implement the forward and generative processes. In VP-SDE, the forward process can be given by:

$$\mathbf{x}_t = \sqrt{\bar{\alpha}(t)}\mathbf{x}_0 + \sqrt{1 - \bar{\alpha}(t)}\mathbf{z}, \quad \mathbf{z} \sim \mathcal{N}(0, \mathbf{I}) \quad (7)$$

where $\alpha(t) := 1 - \beta(t)$ and $\bar{\alpha}(t) := \prod_{s=1}^t \alpha(s)$. And the unique posterior mean of $p(\mathbf{x}_0|\mathbf{x}_t)$ can be obtained through the Tweedie’s approach as follows Efron and Bradley. (2011):

$$\hat{\mathbf{x}}_0 := \mathbb{E}[\mathbf{x}_0|\mathbf{x}_t] = \frac{1}{\sqrt{\bar{\alpha}(t)}} (\mathbf{x}_t + (1 - \bar{\alpha}(t)) \nabla_{\mathbf{x}_t} \log p_t(\mathbf{x}_t)). \quad (8)$$

Since $p(\mathbf{y}|\mathbf{x}_t) \simeq p(\mathbf{y}|\hat{\mathbf{x}}_0)$ Chung et al. (2022a), where $\hat{\mathbf{x}}_0$ is the posterior mean of $p(\mathbf{x}_0|\mathbf{x}_t)$, we modify (5) by approximating $p(\mathbf{y}|\mathbf{x}_t)$ by $p(\mathbf{y}|\hat{\mathbf{x}}_0)$ and approximating $\nabla_{\mathbf{x}_t} \log p_t(\mathbf{x}_t)$ by $s_{\theta^*}(\mathbf{x}_t, t)$. Then, the discrete form of (6) becomes:

$$\mathbf{x}'_{i-1} = \mathbf{f}(\mathbf{x}_i, s_\theta) - \alpha \frac{\partial}{\partial \mathbf{x}_i} \|\mathbf{y} - \mathcal{H}\hat{\mathbf{x}}_0(\bar{\mathbf{x}}_i)\|_2^2 + g(\mathbf{x}_i)\mathbf{z}, \quad \mathbf{z} \sim \mathcal{N}(0, \mathbf{I}) \quad (9)$$

where the choice of $\mathbf{f}(\mathbf{x}_i, s_\theta)$ in VP-SDE is $(\mathbf{x}_i + (1 - \alpha_i)s_\theta(\mathbf{x}_i, i)) / \sqrt{\bar{\alpha}_i}$ and $g(\mathbf{x}_i)$ is $\sqrt{\sigma_i}$, which is a learnable parameter as in Dhariwal et al. (2021).

In addition, MCG imposes the data consistency step to strengthen the measurement consistency:

$$\mathbf{x}_{i-1} = (\mathcal{I} - \mathcal{H}^T \mathcal{H}) \mathbf{x}'_{i-1} + \mathcal{H}^T \mathbf{y}_{i-1}, \quad (10)$$

where $\mathbf{y}_i = \sqrt{\bar{\alpha}_i} \mathbf{y} + \sqrt{1 - \bar{\alpha}_i} \mathbf{z}$, $\mathbf{z} \sim \mathcal{N}(0, \mathbf{I})$. Putting the discretized conditional reverse diffusion step and the data consistency step together, one can sample from $p(\mathbf{x}_t | \mathbf{y})$ by applying (9) and (10). Eventually, the final inpainting output becomes the combination of the last sampled prediction \mathbf{x}'_0 and the measurement \mathbf{y}

$$\mathbf{x}_0 = (\mathcal{I} - \mathcal{H}^T \mathcal{H}) \mathbf{x}'_0 + \mathcal{H}^T \mathbf{y}, \quad (11)$$

Table 1: Data Distribution of CoNSeP and GLySAC

Synthesis	CoNSeP				GLySAC		
	Miscellaneous	Inflammatory	Epithelial	Spindle	Miscellaneous	Inflammation	Epithelial
Baseline	371	3941	5537	5706	3386	7409	7154
NucleiMix (k=200)	569	3938	5457	5690	3586	7356	7091
NucleiMix (k=400)	769	3935	5400	5672	3786	7300	7033
NucleiMix (k=600)	967	3931	5352	5659	3986	7254	6987
NucleiMix (k=800)	1163	3931	5273	5643	4183	7214	6953
CutMix (k=600)	968	3940	5537	5704	3982	7405	7152
CopyPaste (k=600)	970	3941	5537	5706	3985	7409	7152
GradMix (k=600)	971	3772	5306	5506	3986	6998	6965

Table 2: Data Distribution of MoNuSAC

Synthesis	Macrophages				Neutrophils				Macrophages and Neutrophils			
	Epithelial	Lymphocyte	Macrophages	Neutrophils	Epithelial	Lymphocyte	Macrophages	Neutrophils	Epithelial	Lymphocyte	Macrophages	Neutrophils
Baseline	12121	12524	422	541	12121	12524	422	541	12121	12524	422	541
NucleiMix (k=200)	12118	12512	620	540	12091	12478	422	741	12085	12464	623	737
NucleiMix (k=400)	12113	12506	818	540	12053	12445	422	941	12031	12384	822	936
NucleiMix (k=600)	12105	12496	1018	539	12026	12414	422	1141	11951	12350	1027	1128
NucleiMix (k=800)	12096	12493	1217	539	11997	12393	422	1340	11907	12304	1245	1309
CutMix (k=600)	12040	12246	1013	522	12120	12511	422	1140	12036	12187	1015	1071
CopyPaste (k=600)	12077	12337	1015	518	12077	12337	422	1140	12077	12337	1015	1086
GradMix (k=600)	11736	11891	1021	540	11672	12373	422	1141	11347	11680	1021	1140

Algorithm 1 NucleiMix Augmentation

Require: Pathology image dataset \mathcal{D} with a number of rare-type nuclei

$\mathcal{A}^r = \{\alpha_i^r | i = 1, \dots, N_r\}$, major-type nuclei $\mathcal{A}^m = \{\alpha_i^m | i = 1, \dots, N_m\}$,
and background locations $\mathcal{A}^b = \{\alpha_i^b | i = 1, \dots, N_b\}$.

- 1: $\mathcal{P}^r = \{\phi_i^r | i = 1, \dots, N_r\} \leftarrow \text{CropPatch}(\mathcal{A}^r)$
 - 2: $\mathcal{P}^m = \{\phi_i^m | i = 1, \dots, N_m\} \leftarrow \text{CropPatch}(\mathcal{A}^m)$
 - 3: $\mathcal{P}^b = \{\phi_i^b | i = 1, \dots, N_b\} \leftarrow \text{CropPatch}(\mathcal{A}^b)$
▷ Crop patches using \mathcal{A}^r , \mathcal{A}^m , and \mathcal{A}^b .
 - 4: $\mathcal{X}^r = \{x_i^r \in \mathbb{R}^p, i = 1, \dots, N_r\} \leftarrow \text{ExtractFeatures}(\mathcal{P}^r)$
 - 5: $\mathcal{X}^m = \{x_i^m \in \mathbb{R}^p, i = 1, \dots, N_m\} \leftarrow \text{ExtractFeatures}(\mathcal{P}^m)$
 - 6: $\mathcal{X}^b = \{x_i^b \in \mathbb{R}^p, i = 1, \dots, N_b\} \leftarrow \text{ExtractFeatures}(\mathcal{P}^b)$
▷ Extract feature vectors from \mathcal{P}^r , \mathcal{P}^m , and \mathcal{P}^b .
 - 7: Use GMM to model the distribution of $p(\mathcal{P}^r) = p(\mathcal{X}^r) = \mathcal{N}(\mu^r, \Sigma^r)$
 - 8: Predict the conditional joint likelihood of major-type patches and background-type patches $p(\mathcal{P}^m, \mathcal{P}^b | \mathcal{P}^r) = \mathcal{N}(\mathcal{X}^m, \mathcal{X}^b | \mu^r, \Sigma^r)$
 - 9: **for** $j = 1$ to k **do**
 - 10: Sample $\hat{\phi}_j^t \sim p(\mathcal{P}^m, \mathcal{P}^b | \mathcal{P}^r)$, where t is either m or b
 - 11: Sample the most likely rare-type patch $\phi^{r|t} \sim p(\phi_i^r | \hat{\phi}_j^t) = \frac{e^{-w_i \times D(\hat{\phi}_j^t, \phi_i^r)}}{\sum_{k=1}^{N_r} e^{-w_k \times D(\hat{\phi}_j^t, \alpha_k^r)}}$
 - 12: **if** $\hat{\phi}_j^t$ is major-type patch ($t = m$) **then**
 - 13: Copy-and-Replace: copy the α^r at the center of $\phi^{r|m}$ to replace the α^m at the center of ϕ_j^m
 - 14: **else if** $\hat{\phi}_j^t$ is background-type patch ($t = b$) **then**
 - 15: Copy-and-Paste: copy the α^r at the center of $\phi^{r|m}$ to paste at the center of ϕ_j^m
 - 16: **end if**
 - 17: **end for**
-

4. Experiments

4.1. Datasets

4.1.1. Dataset for Diffusion Model Training

A diffusion model is trained on a collection of pathology image patches of 12 different organs from TCGA (<https://github.com/aleju/imgaug>), including 1) 5k bladder urothelial carcinoma; 2) 5k breast invasive carcinoma; 3) 5k cervical squamous cell carcinoma and endocervical adenocarcinoma; 4) 5k colon adenocarcinoma; 5) 2460 kidney chromophobe; 6) 5k liver hepatocellular carcinoma; 7) 5k lung adenocarcinoma; 8) 4090 pancreatic adenocarcinoma; 9) 5k prostate adenocarcinoma; 10) 1880 rectum adenocarcinoma; 11) 5k stomach adenocarcinoma; 12) 1640 uveal melanoma. Each image patch has a spatial size of 256×256 pixels and a resolution of $0.5 \mu\text{m} \times 0.5 \mu\text{m}$ per pixel.

4.1.2. Dataset for Nuclei Instance Segmentation

We employ three public datasets for nuclei instance segmentation such as CoNSeP, GLySAC, and MoNUSAC. Table 1 depicts the details of these datasets.

CoNSeP, which stands for Colorectal Nuclear Segmentation and Phenotypes dataset, was extracted from 16 colorectal adenocarcinoma whole slide images (WSIs) and contains 41 image patches of size 1000×1000 pixels, digitized at $40 \times$ magnification. The dataset has four classes: epithelial, inflammatory, spindle, and miscellaneous. The dataset is partitioned into a training set of 27 images and a testing set of 14 images.

GLySAC, known as Gastric Lymphocyte Segmentation And Classification, was derived from 8 gastric adenocarcinoma WSIs that were digitized at $40 \times$ magnification. This dataset contains 59 image patches, of which 34 patches are designated as the training dataset and the remaining 25 patches are the test dataset. All nuclei in the dataset are classified into three types: lymphocytes, epithelial, and miscellaneous.

MoNuSAC (Multi-organ Nuclei Segmentation And Classification) comprises 209 annotated image patches of size ranging from 81×113 to 1422×2162 pixels. The image patches are split into a training set of 168 patches and a test set of 41 patches. These patches are sourced from various organs, including the breast, kidney, lung, and prostate. The annotated nuclei are grouped into four types: epithelial, lymphocytes, macrophages, and neutrophils.

4.2. Experimental Design

To investigate the effectiveness of NucleiMix, we conduct nuclei instance segmentation with and without data augmentation using NucleiMix and compare the performance between them on the three public datasets (CoNSeP, GLySAC, and MoNuSAC). For each of these datasets, we augment nuclei data by inserting k rare-type nuclei, either in place of major-type nuclei or at the background locations. We set $k = 200, 400, 600,$ and 800 for all three datasets. For nuclei instance segmentation, we employ two popular backbone models SONNET Doan et al. (2022b) and PointNu Yao et al. (2023). Both models are separately trained and evaluated on the augmented datasets with varying k to assess the impact of the augmented instances on the performance. Moreover, we compare NucleiMix with three other data augmentation methods such as CutMix Yun et al. (2019), CopyPaste Ghiasi et al. (2021), and GradMix Doan et al. (2022a). Each of these methods is used in the same manner as NucleiMix to assess the performance of nuclei instance segmentation on the three public datasets.

4.3. Implementation and Training Details

We used 2 RTX6000 GPUs to train a diffusion model with 300k steps using 50,070 image patches of 256×256 pixels, loaded with the 256×256 diffusion pre-trained weight. For image sampling, we applied 250 DDIM steps Song et al. (2020a) and the Manifold Constraint Gradient (MCG) (Chung et al., 2022b) correction term to boost the inpainting performance.

We trained two nuclei segmentation and classification models, SONNET and PointNu, on the original datasets (without data augmentation) for 100 epochs, forming baseline models. Starting from the 50th checkpoint of these baseline models, we trained the two models on the augmented datasets for an additional 50 epochs. All models were trained with Adam optimizer ($\beta_1 = 0.9, \beta_2 = 0.999, \epsilon = 1.0e^{-8}$) and cosine annealing warm restarts scheduler with $eta_{min} = 1.0e^{-5}$ and $T_0 = 25$. The learning rate was initially set to $1.0e^{-4}$, decreasing to $1.0e^{-5}$ after every 25 epochs and restarting from $1.0e^{-4}$. The image patches were resized to 512×512 pixels.

For SONNET, we used 2 RTX6000 GPUs to train a baseline model, with a batch size for each GPU set to 16 for the first 50 epochs and 4 for the second 50 epochs. To train it on the augmented datasets, a batch size for each GPU was set to 4 for 50 epochs. As for PointNu, we used 1 RTX6000 GPU with a batch size of 16. Traditional on-the-fly data augmentation techniques, including random horizontal and vertical flips, Gaussian blurring,

Gaussian noise, color change in hue, saturation, and modification of contrast, were utilized during training. These were implemented using Aleju library (<https://github.com/aleju/imgaug>).

4.4. Evaluation metrics

To evaluate the performance of nuclei segmentation, we employ five evaluation metrics: 1) DICE score to measure the overlap between the predicted segmentation and the ground truth Vu and et al. (2019), 2) Aggregated Jaccard Index (AJI) to measure the accuracy of the nuclei segmentation Kumar et al. (2017b), 3) Detection Quality (DQ) focus on how well the individual objects are detected, 4) Segmentation Quality (SQ) measures how well the segmentation matches the ground truth once the objects are correctly detected, 5) Panoptic Quality (PQ) is a combination of DQ and SQ, robust measurement of how well the objects are detected and how well they are segmented Kirillov et al. (2019). For nuclei classification, we utilized 1) Detection Quality F_d score to measure how well the objects are detected and classified Kirillov et al. (2019), 2) Accuracy (Acc) to measure the proportion of correct predictions, and 3) F_1 score for each nuclei type to measure how well the model identifies positive instances van Rijsbergen and Joost (1979), denote as F_c^t .

Table 3: Results of Nuclei Segmentation on CoNSEP with Augmented Miscellaneous Nuclei

Model	Augmentation	DICE	↑ (%)	AJI	↑ (%)	DQ	↑ (%)	SQ	↑ (%)	PQ	↑ (%)
SONNET	Baseline	0.830±0.001		0.479±0.009		0.632±0.006		0.758±0.002		0.480±0.006	
	NucleiMix (Ours)	0.832 ± 0.001	0.24	0.498 ± 0.006	3.97	0.651 ± 0.005	3.01	0.763 ± 0.002	0.66	0.498 ± 0.006	3.75
	CutMix	0.829±0.001	-0.12	0.488±0.003	1.88	0.641±0.004	1.42	0.760±0.002	0.26	0.488±0.004	1.67
	CopyPaste	0.829±0.001	-0.12	0.481±0.008	0.42	0.637±0.003	0.79	0.762±0.001	0.53	0.486±0.003	1.25
	GradMix	0.829±0.002	-0.12	0.479±0.005	0.00	0.636±0.006	0.63	0.761±0.002	0.40	0.485±0.005	1.04
PointNu	Baseline	0.743±0.005		0.491±0.006		0.665±0.001		0.757±0.002		0.504±0.001	
	NucleiMix (Ours)	0.784 ± 0.004	5.52	0.525 ± 0.001	6.92	0.685 ± 0.004	3.01	0.757±0.002	0.00	0.520 ± 0.005	3.17
	CutMix	0.778±0.010	4.71	0.521±0.008	6.11	0.681±0.009	2.41	0.754±0.002	0.00	0.515±0.008	3.17
	CopyPaste	0.778±0.002	4.71	0.521±0.002	6.11	0.682±0.007	2.56	0.758 ± 0.004	0.13	0.518±0.008	2.78
	GradMix	0.777±0.017	4.58	0.522±0.016	6.31	0.679±0.017	2.11	0.755±0.005	-0.26	0.513±0.016	1.79

5. Results

We explored the impact of augmenting rare-type nuclei on three datasets: CoNSEP Graham et al. (2019), GLySAC Doan et al. (2022b), and MoNuSAC Verma

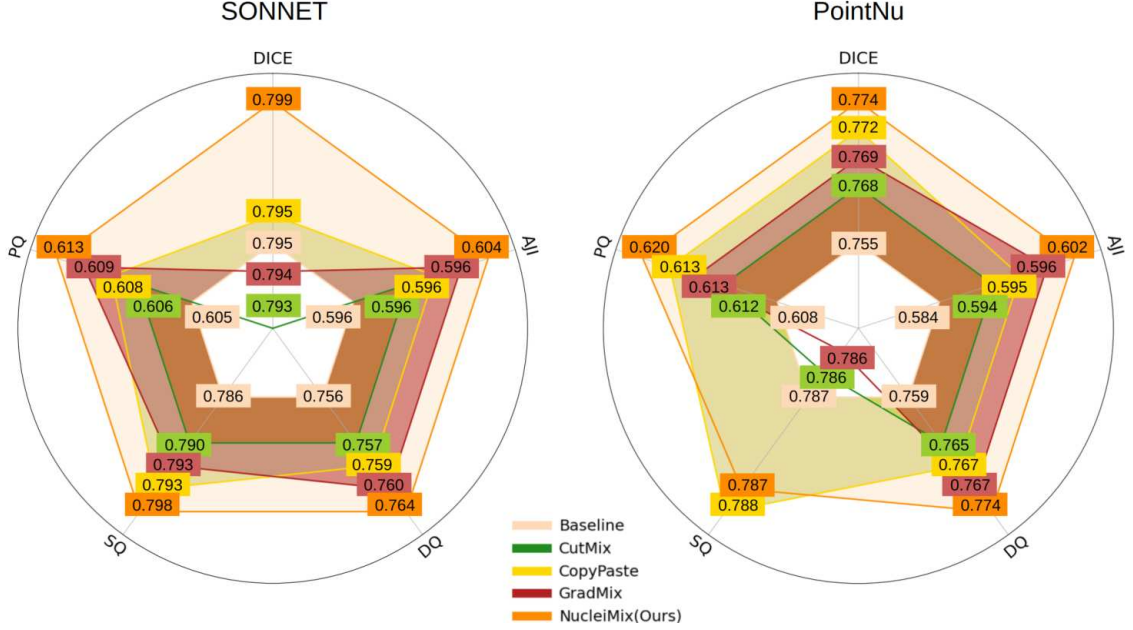


Figure 4: Radar charts for the results of the nuclei segmentation using SONNET and PointNu among baseline, CutMix, CopyPaste, Gradmix and NucleiMix. The numbers represent the average scores across three datasets (CoNSeP, GLySAC, and MoNuSAC).

Table 4: Results of Nuclei Classification on CoNSeP with Augmented Miscellaneous Nuclei

Model	Augmentation	F_d	\uparrow (%)	Acc	\uparrow (%)	F_c^M	\uparrow (%)	F_c^I	\uparrow (%)	F_c^E	\uparrow (%)	F_c^S	\uparrow (%)
SONNET	Baseline	0.741±0.003		0.852±0.003		0.352±0.051		0.595±0.006		0.607±0.010		0.555±0.008	
	NucleiMix (Ours)	0.742 ± 0.002	0.13	0.855 ± 0.002	0.35	0.410 ± 0.041	16.48	0.598 ± 0.016	0.50	0.608 ± 0.004	0.16	0.555 ± 0.005	0.00
	CutMix	0.735±0.001	-0.81	0.852±0.002	0.00	0.348±0.019	-1.14	0.597±0.015	0.34	0.602±0.002	-0.82	0.551±0.004	-0.72
	CopyPaste	0.733±0.007	-1.08	0.854±0.001	0.23	0.354±0.018	0.57	0.582±0.010	-2.18	0.606±0.012	-0.16	0.555±0.006	0.00
	GradMix	0.742±0.004	0.13	0.846±0.003	-0.70	0.380±0.022	7.95	0.593±0.009	-0.34	0.597±0.004	-1.65	0.545±0.009	-1.80
PointNu	Baseline	0.724±0.003		0.888±0.005		0.544±0.021		0.661±0.020		0.620±0.014		0.542±0.014	
	NucleiMix (Ours)	0.744 ± 0.004	2.76	0.897 ± 0.007	1.01	0.600 ± 0.005	10.29	0.680 ± 0.006	2.87	0.651 ± 0.009	5.00	0.558 ± 0.019	2.95
	CutMix	0.738±0.003	1.93	0.890±0.007	0.23	0.590±0.015	8.46	0.665±0.014	0.61	0.644±0.011	3.87	0.542±0.012	0.00
	CopyPaste	0.741±0.005	2.35	0.895±0.003	0.79	0.576±0.005	5.88	0.666±0.008	0.76	0.650±0.008	4.84	0.557±0.004	2.77
	GradMix	0.730±0.024	0.83	0.890±0.005	0.23	0.589±0.013	8.27	0.637±0.021	-3.63	0.632±0.022	1.94	0.556±0.001	2.58

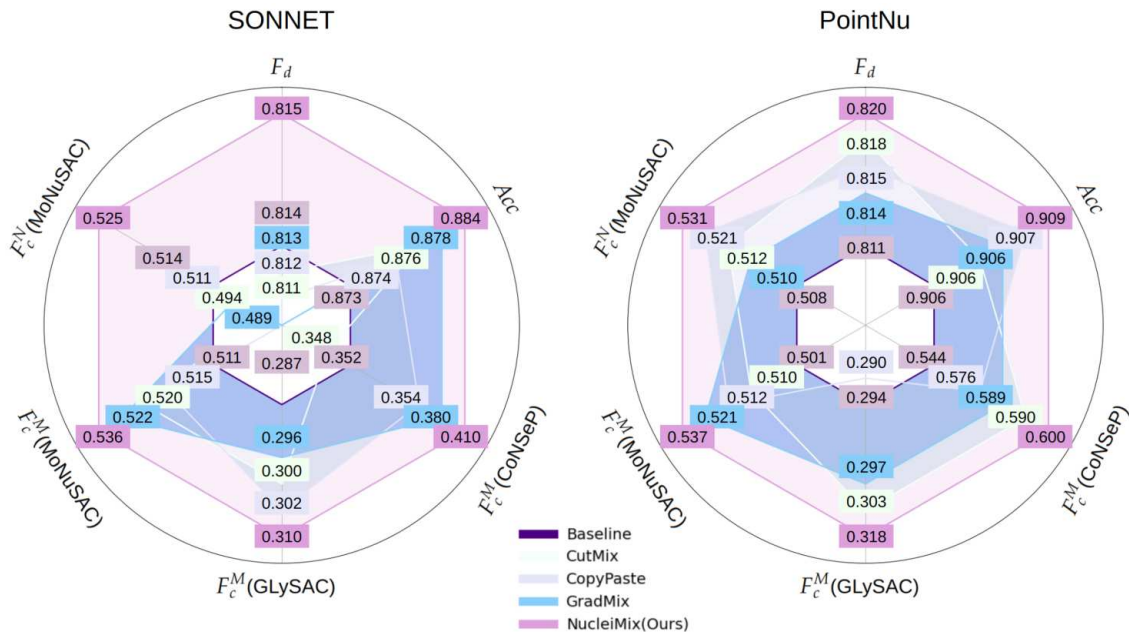


Figure 5: Radar charts for the results of the nuclei classification using SONNET and PointNu among baseline, CutMix, CopyPaste, Gradmix and NucleiMix. The numbers represent the average scores across three datasets (CoNSeP, GLySAC, and MoNuSAC).

Table 5: Results of Nuclei Segmentation on GLySAC with Augmented Miscellaneous Nuclei

Model	Augmentation	DICE	\uparrow (%)	AJI	\uparrow (%)	DQ	\uparrow (%)	SQ	\uparrow (%)	PQ	\uparrow (%)
SONNET	Baseline	0.822±0.002		0.627±0.004		0.786±0.005		0.782±0.002		0.617±0.004	
	NucleiMix (Ours)	0.822±0.000	0.00	0.631 ± 0.001	0.64	0.786±0.004	0.00	0.784 ± 0.002	0.26	0.619 ± 0.002	0.32
	CutMix	0.820±0.002	-0.24	0.628±0.002	0.16	0.786±0.004	0.00	0.783±0.001	0.13	0.618±0.006	0.16
	CopyPaste	0.821±0.002	-0.12	0.629±0.003	0.32	0.787 ± 0.003	0.13	0.782±0.13	0.00	0.618±0.005	0.16
	GradMix	0.823 ± 0.001	0.12	0.629±0.004	0.32	0.784±0.003	-0.25	0.783±0.001	0.13	0.617±0.001	0.00
PointNu	Baseline	0.808±0.001		0.629±0.001		0.800±0.001		0.786 ± 0.000		0.630±0.001	
	NucleiMix (Ours)	0.808±0.001	0.00	0.629±0.001	0.00	0.802 ± 0.001	0.25	0.786±0.001	-0.13	0.631 ± 0.000	0.16
	CutMix	0.811±0.000	0.37	0.630 ± 0.001	0.16	0.798±0.002	-0.25	0.781±0.001	-0.64	0.625±0.002	-0.79
	CopyPaste	0.813 ± 0.001	0.62	0.630 ± 0.001	0.16	0.799±0.002	-0.13	0.782±0.001	-0.51	0.626±0.002	-0.63
	GradMix	0.811±0.004	0.37	0.630±0.005	0.16	0.801±0.003	0.13	0.783±0.001	-0.38	0.629±0.004	-0.16

Table 6: Results of Nuclei Classification on GLySAC with Augmented Miscellaneous Nuclei

Model	Augmentation	F_d	\uparrow (%)	Acc	\uparrow (%)	F_c^M	\uparrow (%)	F_c^L	\uparrow (%)	F_c^E	\uparrow (%)
SONNET	Baseline	0.838±0.003		0.698±0.004		0.287±0.05		0.520±0.007		0.540±0.005	
	NucleiMix (Ours)	0.843 ± 0.004	0.60	0.706 ± 0.005	1.15	0.310 ± 0.011	8.01	0.531 ± 0.013	2.12	0.545 ± 0.003	0.93
	CutMix	0.838±0.002	0.00	0.704±0.003	0.86	0.300±0.008	4.53	0.527±0.009	1.35	0.541±0.006	0.19
	CopyPaste	0.838±0.001	0.00	0.705±0.004	1.00	0.302±0.006	5.23	0.520±0.008	0.00	0.544±0.010	0.74
	GradMix	0.834±0.012	-0.48	0.695±0.015	-0.43	0.296±0.005	3.14	0.510±0.033	-1.92	0.544±0.004	0.74
PointNu	Baseline	0.824±0.002		0.715±0.010		0.294±0.010		0.518±0.019		0.553±0.004	
	NucleiMix (Ours)	0.832±0.005	0.97	0.720 ± 0.006	0.70	0.318 ± 0.004	8.16	0.525 ± 0.005	1.35	0.563 ± 0.010	1.81
	CutMix	0.829±0.004	0.61	0.716±0.008	0.14	0.303±0.008	3.06	0.516±0.011	-0.39	0.557±0.013	0.72
	CopyPaste	0.832±0.005	0.97	0.711±0.011	-0.56	0.290±0.010	-1.36	0.520±0.021	0.39	0.559±0.005	1.08
	GradMix	0.832 ± 0.004	0.97	0.717±0.007	0.28	0.297±0.014	1.02	0.520±0.019	0.39	0.553±0.008	0.00

Table 7: Results of Nuclei Segmentation on MoNuSAC with Augmented Neutrophils

Model	Augmentation	DICE	\uparrow (%)	AJI	\uparrow (%)	DQ	\uparrow (%)	SQ	\uparrow (%)	PQ	\uparrow (%)
SONNET	Baseline	0.774±0.006		0.624±0.006		0.788±0.007		0.797±0.003		0.643±0.004	
	NucleiMix (Ours)	0.778 ± 0.002	0.52	0.627±0.001	0.48	0.792±0.001	0.51	0.819 ± 0.001	2.76	0.650 ± 0.001	1.09
	CutMix	0.777±0.004	0.39	0.629±0.002	0.80	0.791±0.005	0.38	0.800±0.009	0.38	0.644±0.003	0.16
	CopyPaste	0.778 ± 0.002	0.52	0.630±0.003	0.96	0.794±0.004	0.76	0.804±0.012	0.88	0.649±0.005	0.93
	GradMix	0.776±0.001	0.26	0.630 ± 0.002	0.96	0.796 ± 0.004	1.02	0.795±0.002	-0.25	0.648±0.004	0.78
PointNu	Baseline	0.742±0.010		0.600±0.009		0.777±0.009		0.797±0.005		0.635±0.008	
	NucleiMix (Ours)	0.764 ± 0.005	0.52	0.624 ± 0.007	0.48	0.797 ± 0.003	0.51	0.799±0.002	2.76	0.653 ± 0.004	1.09
	CutMix	0.755±0.011	0.39	0.610±0.011	0.80	0.788±0.007	0.38	0.796±0.003	0.38	0.643±0.007	0.16
	CopyPaste	0.760±0.007	0.52	0.616±0.008	0.96	0.789±0.003	0.76	0.801 ± 0.004	0.88	0.647±0.006	0.93
	GradMix	0.756±0.007	0.26	0.612±0.008	0.96	0.784±0.007	1.02	0.797±0.003	-0.25	0.640±0.006	0.78

Table 8: Results of Nuclei Classification on MoNuSAC with Augmented Neutrophils

Model	Augmentation	F_d	\uparrow (%)	Acc	\uparrow (%)	F_c^E	\uparrow (%)	F_c^L	\uparrow (%)	F_c^M	\uparrow (%)	F_c^N	\uparrow (%)
SONNET	Baseline	0.830 ± 0.001		0.939±0.004		0.709±0.005		0.786±0.008		0.511±0.017		0.514 ± 0.028	
	NucleiMix (Ours)	0.827±0.003	-0.36	0.946±0.004	0.75	0.725±0.002	2.26	0.787±0.016	0.13	0.529 ± 0.004	3.52	0.503±0.005	-2.14
	CutMix	0.827±0.003	-0.36	0.947 ± 0.007	0.85	0.728±0.012	2.68	0.787±0.005	0.13	0.522±0.021	2.15	0.486±0.038	-5.45
	CopyPaste	0.830±0.007	0.00	0.945±0.006	0.64	0.725±0.010	2.26	0.794±0.012	1.02	0.524±0.020	2.54	0.490±0.028	-4.67
	GradMix	0.828±0.002	-0.24	0.945±0.015	0.64	0.729 ± 0.011	2.82	0.795 ± 0.011	1.15	0.526±0.025	2.94	0.495±0.030	-3.70
PointNu	Baseline	0.835±0.001		0.975±0.001		0.786±0.004		0.828±0.007		0.501±0.018		0.508±0.036	
	NucleiMix (Ours)	0.839 ± 0.005	0.48	0.976 ± 0.002	0.10	0.794 ± 0.008	1.02	0.829 ± 0.002	0.12	0.534 ± 0.011	6.59	0.538 ± 0.021	5.91
	CutMix	0.830±0.002	-0.60	0.973±0.002	-0.21	0.785±0.002	-0.13	0.818±0.007	-1.21	0.512±0.015	2.20	0.524±0.026	3.15
	CopyPaste	0.835±0.001	0.00	0.975±0.001	0.00	0.788±0.003	0.25	0.826±0.006	-0.24	0.526±0.001	4.99	0.529±0.014	4.13
	GradMix	0.833±0.004	-0.24	0.975±0.001	0.00	0.789±0.005	0.38	0.822±0.001	-0.72	0.525±0.018	4.79	0.529±0.024	4.13

Table 9: Results of Nuclei Segmentation on MoNuSAC with Augmented Macrophages

Model	Augmentation	DICE	↑ (%)	AJI	↑ (%)	DQ	↑ (%)	SQ	↑ (%)	PQ	↑ (%)
SONNET	Baseline	0.774±0.006		0.624±0.006		0.788±0.007		0.797±0.003		0.643±0.004	
	NucleiMix (Ours)	0.782 ± 0.001	1.03	0.630 ± 0.004	0.96	0.795 ± 0.005	0.89	0.816±0.003	2.38	0.650 ± 0.004	1.09
	CutMix	0.767±0.003	-0.90	0.612±0.002	-1.92	0.783±0.004	-0.63	0.805±0.010	1.00	0.637±0.003	-0.93
	CopyPaste	0.771±0.005	-0.39	0.616±0.006	-1.28	0.785±0.006	-0.38	0.808±0.011	1.38	0.642±0.005	-0.16
	GradMix	0.772±0.002	-0.26	0.622±0.000	-0.32	0.792±0.002	0.51	0.818 ± 0.002	2.63	0.648±0.001	0.78
PointNu	Baseline	0.742±0.010		0.600±0.009		0.777±0.009		0.797±0.005		0.635±0.008	
	NucleiMix (Ours)	0.756 ± 0.004	1.89	0.614 ± 0.004	2.33	0.790 ± 0.006	1.67	0.799±0.004	0.25	0.647 ± 0.002	1.89
	CutMix	0.747±0.002	0.67	0.603±0.002	0.50	0.778±0.003	0.13	0.798±0.002	0.13	0.636±0.003	0.16
	CopyPaste	0.750±0.009	1.08	0.601±0.013	0.17	0.778±0.008	0.13	0.796±0.004	-0.13	0.634±0.009	-0.16
	GradMix	0.755±0.002	1.75	0.612±0.008	2.00	0.787±0.005	1.29	0.799 ± 0.001	0.25	0.644±0.003	1.42

Table 10: Results of Nuclei Classification on MoNuSAC with Augmented Macrophages

Model	Augmentation	F_d	↑ (%)	Acc	↑ (%)	F_c^E	↑ (%)	F_c^L	↑ (%)	F_c^M	↑ (%)	F_c^N	↑ (%)
SONNET	Baseline	0.830±0.001		0.939±0.004		0.709±0.005		0.786±0.008		0.511±0.017		0.514±0.028	
	NucleiMix (Ours)	0.835 ± 0.002	0.60	0.952 ± 0.007	1.38	0.746 ± 0.010	5.22	0.801 ± 0.006	1.91	0.532 ± 0.009	4.11	0.535 ± 0.019	4.09
	CutMix	0.830±0.008	0.00	0.940±0.007	0.11	0.710±0.003	0.14	0.790±0.008	0.51	0.516±0.005	0.98	0.485±0.016	-5.64
	CopyPaste	0.830±0.005	0.00	0.937±0.004	-0.21	0.718±0.005	1.27	0.778±0.001	-1.02	0.514±0.022	0.59	0.532±0.006	3.50
	GradMix	0.831±0.001	0.12	0.947±0.000	0.85	0.730±0.000	2.96	0.800±0.001	1.78	0.513±0.022	0.39	0.494±0.004	-3.89
PointNu	Baseline	0.835±0.001		0.975±0.001		0.786±0.004		0.828±0.007		0.501±0.018		0.508±0.036	
	NucleiMix (Ours)	0.840 ± 0.006	0.60	0.976 ± 0.001	0.10	0.796 ± 0.006	1.27	0.832 ± 0.003	0.48	0.545 ± 0.003	8.78	0.528 ± 0.008	3.94
	CutMix	0.835±0.005	0.00	0.975±0.003	0.00	0.786±0.010	0.00	0.827±0.008	-0.12	0.507±0.024	1.20	0.500±0.006	-1.57
	CopyPaste	0.831±0.008	-0.48	0.976±0.001	0.10	0.790±0.002	0.51	0.823±0.013	-0.60	0.507±0.021	1.20	0.516±0.043	1.57
	GradMix	0.838±0.003	0.36	0.975±0.002	0.00	0.792±0.003	0.76	0.829±0.004	0.12	0.531±0.021	5.99	0.492±0.012	-3.15

Table 11: Results of Nuclei Segmentation on MoNuSAC with Augmented Macrophages and Neutrophils

Model	Augmentation	DICE	↑ (%)	AJI	↑ (%)	DQ	↑ (%)	SQ	↑ (%)	PQ	↑ (%)
SONNET	Baseline	0.774±0.006		0.624±0.006		0.788±0.007		0.797±0.003		0.643±0.004	
	NucleiMix (Ours)	0.781 ± 0.005	0.90	0.632 ± 0.007	1.28	0.794 ± 0.008	0.76	0.809±0.006	1.51	0.649 ± 0.004	0.93
	CutMix	0.772±0.005	-0.26	0.622±0.007	-0.32	0.785±0.005	-0.38	0.803±0.008	0.75	0.646±0.008	0.47
	CopyPaste	0.774±0.008	0.00	0.624±0.009	0.00	0.790±0.010	0.25	0.810 ± 0.008	1.63	0.646±0.008	0.47
	GradMix	0.772±0.004	-0.26	0.622±0.004	-0.32	0.792±0.001	0.51	0.808±0.008	1.38	0.647±0.002	0.62
PointNu	Baseline	0.742±0.010		0.600±0.009		0.777±0.009		0.797±0.005		0.635±0.008	
	NucleiMix (Ours)	0.757 ± 0.000	2.02	0.616 ± 0.002	2.67	0.795 ± 0.002	2.32	0.796±0.004	-0.13	0.649 ± 0.002	2.20
	CutMix	0.749±0.011	0.94	0.605±0.011	0.83	0.780±0.004	0.39	0.800±0.001	0.38	0.639±0.004	0.63
	CopyPaste	0.757±0.004	2.02	0.609±0.004	1.50	0.785±0.004	1.03	0.803 ± 0.009	0.75	0.642±0.004	1.10
	GradMix	0.748±0.009	0.81	0.603±0.011	0.50	0.786±0.006	1.16	0.796±0.003	-0.13	0.641±0.007	0.94

Table 12: Results of Nuclei Classification on MoNuSAC with Augmented Macrophages and Neutrophils

Model	Augmentation	F_d	\uparrow (%)	Acc	\uparrow (%)	F_c^R	\uparrow (%)	F_c^L	\uparrow (%)	F_c^M	\uparrow (%)	F_c^N	\uparrow (%)
SONNET	Baseline	0.830 ± 0.001		0.939±0.004		0.709±0.005		0.786±0.008		0.511±0.017		0.514±0.028	
	NucleiMix (Ours)	0.830 ± 0.001	0.00	0.954 ± 0.003	1.60	0.740 ± 0.018	4.37	0.802 ± 0.007	2.04	0.548 ± 0.014	7.24	0.538 ± 0.006	4.67
	CutMix	0.825±0.005	-0.60	0.943±0.004	0.43	0.720±0.007	1.55	0.781±0.004	-0.64	0.521±0.003	1.96	0.511±0.040	-0.58
	CopyPaste	0.828±0.002	-0.24	0.937±0.004	-0.21	0.704±0.004	-0.71	0.784±0.005	-0.25	0.508±0.007	-0.59	0.513±0.015	-0.19
	GradMix	0.829±0.005	-0.12	0.951±0.002	1.28	0.738±0.003	4.09	0.798±0.003	1.53	0.526±0.019	2.94	0.478±0.038	-7.00
PointNu	Baseline	0.835±0.001		0.975±0.001		0.786±0.004		0.828±0.007		0.501±0.018		0.508±0.036	
	NucleiMix (Ours)	0.844 ± 0.002	1.08	0.974±0.003	-0.10	0.799±0.008	1.65	0.829±0.007	0.12	0.534 ± 0.018	6.59	0.530 ± 0.013	4.33
	CutMix	0.839±0.008	0.48	0.977 ± 0.001	0.21	0.799 ± 0.005	1.65	0.831 ± 0.008	0.36	0.512±0.014	2.20	0.512±0.014	0.79
	CopyPaste	0.836±0.006	0.12	0.976±0.002	0.10	0.789±0.009	0.38	0.829±0.010	0.12	0.503±0.023	0.40	0.519±0.008	2.17
	GradMix	0.836±0.006	0.12	0.975±0.001	0.00	0.793±0.004	0.89	0.825±0.008	-0.36	0.506±0.012	1.00	0.510±0.011	0.39

et al. (2021). We use k to denote the number of synthesized nuclei added to the original dataset. In CoNSeP and GLySAC, there is only one type of rare-type nuclei, which is miscellaneous. k number of new miscellaneous nuclei were generated and added to each of the datasets. In the case of MoNuSAC, there are two types of rare-type nuclei: neutrophils and macrophages. We generated three kinds of augmented datasets: 1) only adding k synthesized neutrophils; 2) only adding k synthesized macrophages; 3) adding k synthesized macrophages and k synthesized neutrophils together. The details of the original and augmented datasets are available in Table 1 and 2. We compared NucleiMix with three other methods: CutMix Yun et al. (2019), CopyPaste Ghiasi et al. (2021), and GradMix Doan et al. (2022a) and evaluated the nuclei segmentation and classification performance with and without the augmented datasets on two popular models: SONNET Doan et al. (2022b) and PointNu Yao et al. (2023).

Fig. 4 demonstrates the average performance of nuclei segmentation for SONNET and PointNu using NucleiMix, the baseline (without augmentation), and other augmentation methods (CutMix, CopyPaste, and GradMix) across the three datasets (CoNSeP, GLySAC, and MoNuSAC). In comparison to the baseline and the three augmentation methods, the strength of NucleiMix was prominent. For both SONNET and PointNu, the adoption of NucleiMix, on average, achieved the best performance in all evaluation metrics except SQ for PointNu. For example, using NucleiMix, SONNET obtained 0.799 DICE, 0.604 AJI, 0.764 DQ, 0.798 SQ, and 0.613 PQ, while PointNu attained 0.774 DICE, 0.602 AJI, 0.774 DQ, 0.787 SQ, and 0.620 PQ. Among the three other augmentation methods, CopyPaste and GradMix were comparable to each other, achieving the second or third-best performance in most

of the evaluation metrics. PointNu with CopyPaste, in particular, achieved the highest SQ of 0.788 but obtained the second-best DICE and PQ and third-best AJI and DQ. CutMix was shown to be the poorest among the augmentation methods. Without data augmentation (baseline), both SONNET and PointNu attained the worst performance in all evaluation metrics except DICE for SONNET and SQ for PointNu.

Moreover, we measured and averaged the results of nuclei classification for SONNET and PointNu with and without augmentation methods across the three datasets (Fig. 5). NucleiMix outperformed other augmentation methods as well as the baseline for both SONNET and PointNu. With SONNET, it achieved 0.815 F_d , 0.884 Acc, 0.410 F_c^M in CoNSeP, 0.310 F_c^M in GLySAC, 0.536 F_c^M in MoNuSAC, and 0.525 F_c^N in MoNuSAC. With PointNu, it obtained 0.820 F_d , 0.909 Acc, 0.600 F_c^M in CoNSeP, 0.318 F_c^M in GLySAC, 0.537 F_c^M in MoNuSAC, and 0.531 F_c^N in MoNuSAC. The performance of the other three augmentation methods varied depending on the evaluation metrics, and thus there was no clear second-best-performing model. The baseline was, on the other hand, generally inferior to NucleiMix and other augmentation methods.

We also visually investigated the results of nuclei segmentation and classification using NucleiMix, comparing it with the baseline and three other augmentation methods. Fig. 6 and 7 depict the results of nuclei segmentation and classification using SONNET and PointNu, respectively. Regardless of the backbone models, NucleiMix consistently provided improved segmentation and classification results. For CoNSeP and GLySAC, both NucleiMix and other augmentation methods generally produced segmentation results similar to the ground truth. However, the other augmentation methods often failed to segment rare-type nuclei or over-segmented the nuclei. Similar observations were made in MoNuSAC. Specifically, for macrophages, the other augmentation methods struggled to segment them properly, likely due to their large size, resulting in a tendency to either segment and classify smaller regions or miss them entirely.

5.1. CoNSeP: Augmentation of Miscellaneous Nuclei

Table 3 shows the results of nuclei segmentation on CoNSeP using SONNET and PointNu with and without synthesized miscellaneous nuclei. For both models, NucleiMix provided a substantial performance gain across five evaluation metrics, achieving the best results except SQ for PointNu. In comparison to the baseline, NucleiMix improved SONNET by 0.24% in DICE,

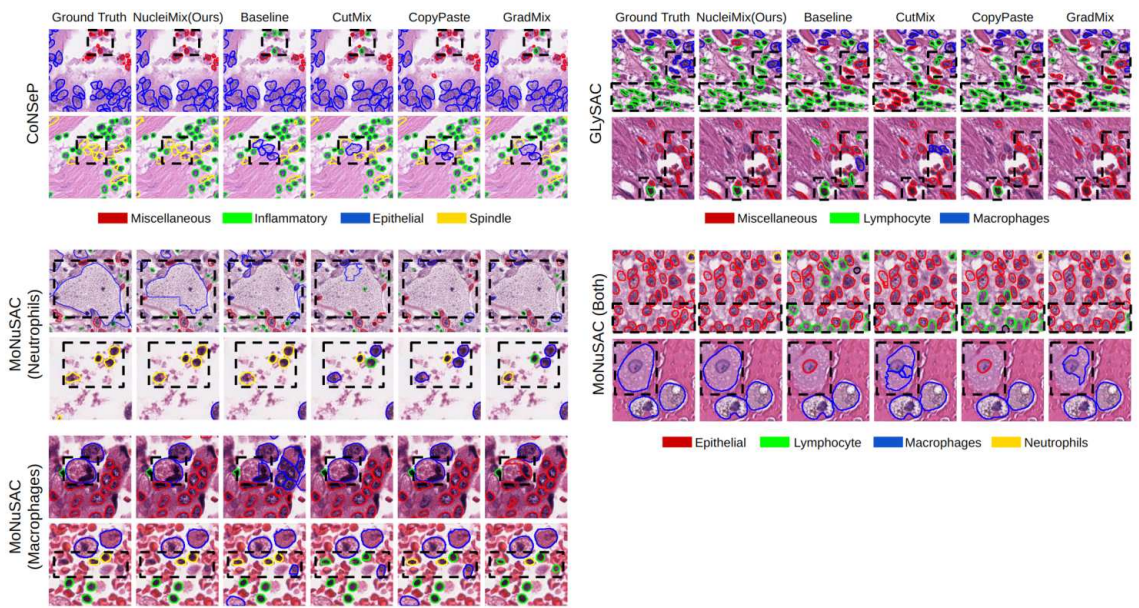


Figure 6: Visual assessment of nuclei segmentation and classification using SONNET

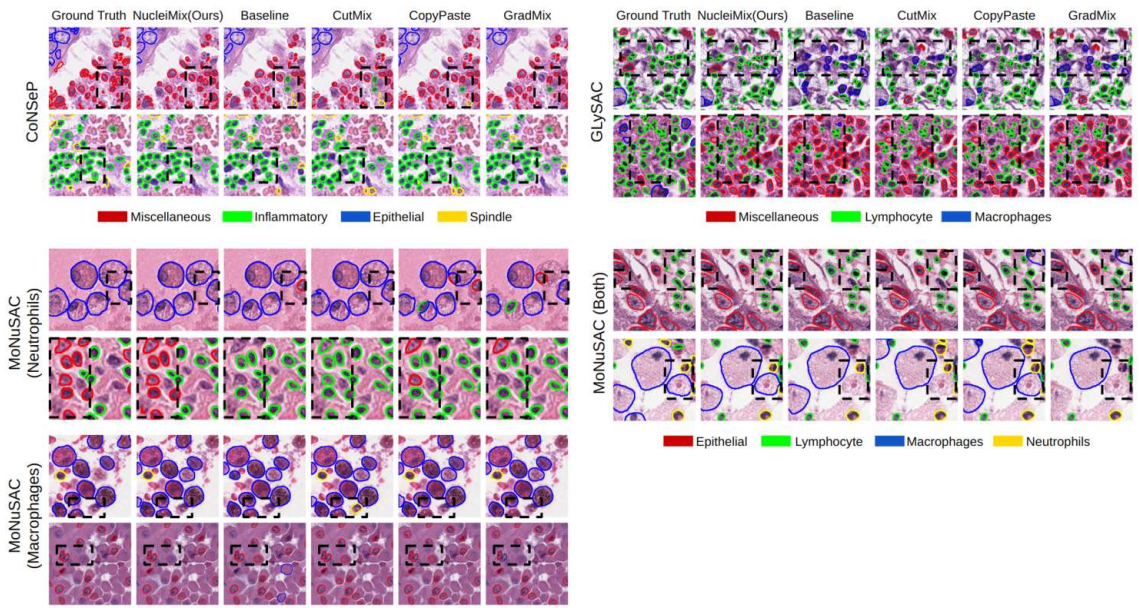


Figure 7: Visual assessment of nuclei segmentation and classification using PointNu

3.97% in AJI, 3.01% in DQ, 0.66% in SQ, and 3.75% in PQ. Similarly, it enhanced PointNu by 5.52% in DICE, 6.92% in AJI, 3.01% in DQ, and 3.17% in PQ. The other three augmentation methods generally improved performance over the baseline but were inferior to NucleiMix.

Table 4 demonstrates the nuclei classification results on CoNSeP for both models. NucleiMix achieved the best performance regardless of evaluation metrics and nuclei classification models. In particular, it substantially improved F_c^M by 16.48% and 10.29% for SONNET and PointNu, respectively, as compared to the baseline, indicating its effectiveness in augmenting rare-type nuclei. The effect of the other augmentation methods was disproportionate across different evaluation metrics and models. For instance, GradMix with SONNET and PointNu increased F_c^M by 7.95% with and 8.27%, respectively; however F_c^I was dropped by 3.63% with PointNu, and F_1 for all other three types (F_c^I , F_c^E , and F_c^S) decreased with SONNET. Similarly, using SONNET, CutMix, and CopyPaste showed worse performance than the baseline, and with PointNu, they obtained lower improvements compared to NucleiMix.

5.2. GLySAC Dataset: Augmentation of Miscellaneous Nuclei

The results of nuclei segmentation, both with and without augmented miscellaneous nuclei, are reported in Table 5. NucleiMix was generally comparable or superior to the baseline and other three augmentation methods for both SONNET and PointNu. For instance, NucleiMix obtained the highest AJI of 0.631, SQ of 0.784, and PQ of 0.619 with SONNET and the best DQ of 0.802 and PQ of 0.631 with PointNu. The performance of the other three augmentation methods was inconsistent across evaluation metrics. CopyPaste achieved the highest DQ of 0.787 with SONNET and the highest DICE and AJI of 0.813 and 0.630, respectively, with PointNu; however, DICE for SONNET and DQ, SQ, and PQ for PointNu were dropped compared to the baseline. GradMix, CutMix, and baseline excelled in only one evaluation metric (GradMix: 0.823 DICE with SONNET; CutMix: 0.630 AJI with PointNu; Baseline: 0.786 SQ with PointNu).

In the nuclei classification on GLySAC (Table 6), the superiority of NucleiMix was apparent. NucleiMix outperformed the baseline and other three augmentation methods except F_d for PointNu. The improvement by NucleiMix varied across different types of nuclei, with the greatest improvement observed for miscellaneous nuclei, achieving an increase of 8.01% with SONNET and 8.16% with PointNu. Although GradMix showed superior performance in F_d with PointNu, it showed worse performance in all other metrics than

NucleiMix. The other two augmentation methods (CutMix and CopyPaste) generally showed improvements over the baseline but exhibited declines in certain metrics.

5.3. MoNuSAC Dataset: Augmentation of Neutrophils

With augmented neutrophils, the nuclei segmentation results on MoNuSAC are presented in Table 7. NucleiMix outperformed the baseline across all evaluation metrics, with improvements ranging from 0.48% to 2.76%. As compared to the other three augmentation methods, NucleiMix generally achieved the highest scores, except for AJI and DQ with SONNET and SQ with PointNu. In regard to the other three augmentation methods, there was no clear second-best method. For example, with SONNET, GradMix obtained the best AJI and DQ of 0.630 and 0.796, respectively, and Copy-Paste demonstrated the highest DICE of 0.778 with SONNET (matching the performance of NucleiMix) and the highest SQ of 0.801 with PointNu. However, their performance across other evaluation metrics was inconsistent.

Table 8 demonstrates the results of nuclei classification on MoNuSAC with augmented neutrophils. The performance of NucleiMix was susceptible to the choice of the backbone model. As paired with PointNu, NucleiMix exhibited the highest scores across all evaluation metrics; however, with SONNET, it only excelled in F_1 for macrophages, and no other method demonstrated consistent superiority with SONNET. For example, the baseline obtained the highest scores for the overall F_d (0.830) and F_c^N (0.514). GradMix showed the best F_1 scores for F_c^E (0.729) and F_c^L (0.795). CutMix recorded the highest Acc (0.947). It was noteworthy that no augmentation method surpassed the baseline F_c^N .

5.4. MoNuSAC Dataset: Augmentation of Macrophages

We demonstrate the results of nuclei segmentation on MoNuSAC with augmented macrophages in Table 9. NucleiMix outperformed the baseline across all evaluation metrics, with improvements ranging from 0.89% to 2.38%, irrespective of the backbone model. As compared to other augmentation methods, NucleiMix demonstrated superior performance across all evaluation metrics, except SQ with both models. The performance of the other three augmentation methods was inconsistent across both evaluation metrics and backbone models. With SONNET, in particular, they were generally inferior to the baseline. The results of nuclei classification on MoNuSAC with augmented macrophages are detailed in Table 10. NucleiMix was superior to

the baseline as well as the three augmentation methods, achieving the highest scores across all evaluation metrics. Notably, concerning F_1 for macrophages, NucleiMix provided substantial performance gains, with increases of 4.11% and 8.78% increase when using SONNET and PointNu, respectively. While the other three augmentation methods also improved F_c^M compared to the baseline, their improvements were smaller than those obtained by NucleiMix, and, in some cases, they obtained worse performance than the baseline on certain evaluation metrics.

5.5. MoNuSAC Dataset: Augmentation of Neutrophils and Macrophages

Table 11 presents the results of nuclei segmentation on MoNuSAC with augmented neutrophils and macrophages. For both backbone models, NucleiMix, by and large, outperformed the baseline and the other three augmentation methods. It provided substantial improvements across most evaluation metrics, achieving the highest scores for DICE, AJI, DQ, and PQ. While CopyPaste obtained the best SQ scores for both models, its performance was inferior to NucleiMix for all other metrics. The other two augmentation methods not only performed worse than NucleiMix but also fell below the baseline on certain metrics.

In the nuclei classification of MoNuSAC with augmented neutrophils and macrophages (Table 12), NucleiMix was shown to be the top-performing method compared to the baseline and the other three augmentation methods. With SONNET, NucleiMix achieved the top scores across all evaluation metrics. Similarly, with PointNu, it obtained the best scores in three evaluation metrics (F_d , F_c^M , and F_c^N) and the second-best scores for F_c^L and F_c^E . It is noteworthy that NucleiMix provided substantial improvements over the baseline for macrophages and neutrophils, increasing F_c^M and F_c^N by 7.24% and 4.67% with SONNET, and by 6.59% and 4.33% with PointNu, respectively.

5.6. Ablation Study: Effect of Number of Augmented Nuclei on Nuclei Segmentation

To investigate the effect of the number of augmented rare-type nuclei, we repeated the nuclei segmentation experiments with varying k for each dataset. The results of nuclei segmentation on CoNSeP with augmented miscellaneous nuclei, GLySAC with augmented miscellaneous nuclei, and MoNuSAC with augmented neutrophils, macrophages, and both macrophages and neutrophils are available in Table 13, 14, 15, 16, and 17, respectively.

On CoNSEP, the addition of synthesized miscellaneous generally provided a performance gain over the baseline across all evaluation metrics, regardless of the number of augmented miscellaneous nuclei. With SONNET, the best performance was achieved when $k=600$, with the improvements ranging from 0.24% to 3.97%, while, with PointNu, it was $k=400$, which yielded the highest scores for DICE (0.785), DQ (0.689), SQ (0.760), and PQ (0.525).

On GLySAC, the impact of the augmented miscellaneous nuclei varied depending on the backbone models. With SONNET, NucleiMix consistently outperformed the baseline across all evaluation metrics, irrespective of the number of augmented nuclei, except for DQ at $k=200$. The optimal performance was observed at $k=400$. In contrast, with PointNu, the performance decreased at both $k=200$ and $k=400$. While the highest improvements in DICE (0.809), AJI (0.630), and DQ (0.803) were acquired at $k=800$, the highest PQ (0.631) was achieved at $k=600$.

On MoNuSAC, the addition of synthesized nuclei clearly enhanced the quality of nuclei segmentation. By augmenting neutrophils alone, both models demonstrated superior performance compared to the baseline across all evaluation metrics. With SONNET, the highest scores for DICE, AJI, and PQ were achieved at $k=200$, with improvements ranging from 0.90% to 1.60%. With PointNu, the best performance across all evaluation metrics, except SQ, was obtained at $k=600$, showing improvements between 2.57% and 4.00%. Similarly, with respect to macrophages, NucleiMix consistently improved the performance of nuclei segmentation with a varying number of augmented macrophages, regardless of backbone models, except for DQ with SONNET when $k=800$. Using SONNET, the highest DQ and PQ were achieved at $k=200$ and the highest DICE and SQ were obtained at $k=600$. For PointNu, the best scores were attained at $k=400$ across all evaluation metrics, which improves upon the performance between 0.38% and 4.00%. As for augmenting both macrophages and neutrophils, the strength of NucleiMix was also evident. Varying k , the segmentation performance was consistently improved compared to the baseline across all evaluation metrics, except for DICE with SONNET at $k=200$ and for SQ with PointNu at $k=600$ and $k=800$. With SONNET, the highest improvements were acquired for DQ, SQ, and PQ with gains of 0.89%, 1.88%, and 1.40%, respectively, at $k=200$, and at $k=600$ for DICE (0.90%) and AJI (1.28%). Using PointNu, when $k=600$, the greatest improvements of 2.67%, 2.32%, and 2.20% were obtained for AJI, DQ, and PQ, respectively, while DICE and SQ enhanced by 2.16% and 0.38% at $k=200$.

5.7. Ablation Study: Effect of Number of Augmented Nuclei on Nuclei Classification

By augmenting rare-type nuclei, we also conducted the nuclei classification experiments with differing k for each dataset. Table 18, 19, 20, 21, and 22 illustrates the results of nuclei classification on CoNSEP with augmented miscellaneous nuclei, GLySAC with augmented miscellaneous nuclei, and MoNuSAC with augmented neutrophils, macrophages, and both macrophages and neutrophils, respectively. The inclusion of synthesized rare-type nuclei generally improved classification performance regardless of the number of augmented nuclei and the type of nuclei. In particular, in most cases, the classification performance of rare-type nuclei showed substantial improvement.

On CoNSEP, SONNET achieved the highest scores for F_d , F_c^M , and F_c^E at $k=400$, Acc and F_c^S at $k=600$, and F_c^I at $k=200$. Meanwhile, PointNu obtained the best scores for Acc , F_c^M , and F_c^I at $k=600$, F_d and F_c^E at $k=400$, and F_c^S at $k=800$. The greatest improvements for miscellaneous nuclei (F_c^M) were observed at $k=400$ with SONNET and at $k=600$ with PointNu, with improvements of 19.89% and 10.29%, respectively, compared to the baseline.

On GLySAC, using SONNET, NucleiMix attained the most substantial improvements for F_d and F_c^E at $k=400$, Acc at $k=200$, and F_c^M and F_c^L at $k=600$. PointNu benefited the most from NucleiMix at $k=800$, achieving the highest F_d , Acc , F_c^L , and F_c^E . In regard to miscellaneous nuclei, the highest F_c^M was obtained at $k=600$ for both models, with enhancements of $\geq 8.01\%$.

On MoNuSAC, augmenting neutrophils alone led to the highest scores with SONNET at $k=200$ across all evaluation metrics except for F_d . As for PointNu, the best scores were split between $k=200$ (Acc , F_c^E , and F_c^N) and $k=800$ (F_d , F_c^L , and F_c^M). The neutrophil nuclei class showed the most improvement for SONNET and PointNu at $k=200$ by 3.50% and 8.27%, respectively. With the augmented macrophages only, $k=400$ and $k=600$ proved to be the most beneficial for SONNET, yielding the highest scores for metrics such as F_d , F_c^M , and F_c^N at $k=400$ and Acc , F_c^E , and F_c^L at $k=600$. For PointNu, $k=600$ was superior to others, resulting in the highest scores for F_c^E , F_c^M , and F_c^N . In the macrophages nuclei category, the best scores of 0.565 and 0.545 were achieved by SONNET at $k=400$ and PointNu at $k=600$, respectively. Including both synthesized neutrophils and macrophages, both models, by and large, performed best at $k=600$; for instance, the most improvements were obtained for SONNET in Acc (1.60%), F_c^E (4.37%), F_c^L

(2.04%), F_c^M (7.24%), and F_c^N (4.67%) and for PointNu in F_d (1.08%), F_c^E (1.65%), F_c^M (6.59%), and F_c^N (4.33%).

Table 13: Effect of Augmented Miscellaneous Nuclei for Nuclei Segmentation on CoNSeP

Model	Augmentation	DICE	↑ (%)	AJI	↑ (%)	DQ	↑ (%)	SQ	↑ (%)	PQ	↑ (%)
SONNET	Baseline	0.830±0.001		0.479±0.009		0.632±0.006		0.758±0.002		0.480±0.006	
	k=200	0.830±0.001	0.00	0.482±0.003	0.63	0.641±0.002	1.42	0.763±0.004	0.66	0.480±0.006	0.00
	k=400	0.832 ± 0.001	0.24	0.495±0.005	3.34	0.647±0.005	2.37	0.763 ± 0.002	0.66	0.495±0.005	3.13
	k=600	0.832 ± 0.001	0.24	0.498 ± 0.006	3.97	0.651 ± 0.005	3.01	0.763 ± 0.002	0.66	0.498 ± 0.006	3.75
	k=800	0.829±0.001	-0.12	0.486±0.005	1.46	0.640±0.000	1.27	0.761±0.001	0.40	0.488±0.001	1.67
PointNu	Baseline	0.743±0.005		0.491±0.006		0.665±0.001		0.757±0.002		0.504±0.001	
	k=200	0.772±0.009	3.90	0.517±0.006	5.30	0.683±0.007	2.71	0.758±0.003	0.13	0.520±0.006	3.17
	k=400	0.785 ± 0.005	5.65	0.523±0.006	6.52	0.689 ± 0.002	3.61	0.760 ± 0.002	0.40	0.525 ± 0.002	4.17
	k=600	0.784±0.004	5.52	0.525 ± 0.001	6.92	0.685±0.004	3.01	0.757±0.002	0.00	0.520±0.005	3.17
	k=800	0.781±0.005	5.11	0.522±0.004	6.31	0.680±0.006	2.26	0.755±0.005	-0.26	0.514±0.008	1.98

Table 14: Effect of Augmented Miscellaneous Nuclei for Nuclei Segmentation on GLySAC

Model	Augmentation	DICE	↑ (%)	AJI	↑ (%)	DQ	↑ (%)	SQ	↑ (%)	PQ	↑ (%)
SONNET	Baseline	0.822±0.002		0.627±0.004		0.786±0.005		0.782±0.002		0.617±0.004	
	k=200	0.823±0.001	0.12	0.632±0.002	0.80	0.785±0.002	-0.13	0.785 ± 0.001	0.38	0.619±0.002	0.32
	k=400	0.824 ± 0.001	0.24	0.634 ± 0.004	1.12	0.788 ± 0.005	0.25	0.785 ± 0.001	0.38	0.621 ± 0.004	0.65
	k=600	0.822±0.000	0.00	0.631±0.001	0.64	0.786±0.004	0.00	0.784±0.002	0.26	0.619±0.002	0.32
	k=800	0.823±0.001	0.12	0.632±0.002	0.80	0.787±0.004	0.13	0.785 ± 0.001	0.38	0.620±0.004	0.49
PointNu	Baseline	0.808±0.001		0.629±0.001		0.800±0.001		0.786 ± 0.000		0.630±0.001	
	k=200	0.805±0.003	-0.37	0.624±0.002	-0.79	0.799±0.002	-0.13	0.782±0.002	-0.51	0.626±0.003	-0.63
	k=400	0.806±0.003	-0.25	0.623±0.005	-0.95	0.797±0.006	-0.38	0.781±0.001	-0.64	0.624±0.005	-0.95
	k=600	0.808±0.001	0.00	0.629±0.001	0.00	0.802±0.001	0.25	0.786±0.001	-0.13	0.631 ± 0.000	0.16
	k=800	0.809 ± 0.004	0.12	0.630 ± 0.003	0.16	0.803 ± 0.002	0.38	0.782±0.002	-0.51	0.629±0.002	-0.16

6. Discussion

Data augmentation techniques are widely used to address data imbalance and to overcome the limitations of small datasets. Mix-based data augmentation methods typically blend parts from existing images to generate composite images. In the context of nuclei instance segmentation, such methods can be adopted to increase the representation of rare-type nuclei. For instance, CutMix and CopyPaste randomly select and paste nuclei to artificially increase the number of rare-type nuclei. GradMix, on the other hand, adopts a more targeted approach, selecting pairs of major-type and

Table 15: Effect of Augmented Neutrophils for Nuclei Segmentation on MoNuSAC

Model	Augmentation	DICE	↑ (%)	AJI	↑ (%)	DQ	↑ (%)	SQ	↑ (%)	PQ	↑ (%)
SONNET	Baseline	0.774±0.006		0.624±0.006		0.788±0.007		0.797±0.003		0.643±0.004	
	k=200	0.781 ± 0.003	0.90	0.634 ± 0.001	1.60	0.794±0.001	0.76	0.814±0.009	2.13	0.651 ± 0.001	1.24
	k=400	0.778±0.007	0.52	0.630±0.005	0.96	0.791±0.002	0.38	0.820 ± 0.001	2.89	0.649±0.001	0.93
	k=600	0.778±0.002	0.52	0.627±0.001	0.48	0.792±0.001	0.51	0.819±0.001	2.76	0.650±0.001	1.09
	k=800	0.779±0.005	0.65	0.628±0.001	0.64	0.795 ± 0.005	0.89	0.807±0.009	1.25	0.647±0.002	0.62
PointNu	Baseline	0.742±0.010		0.600±0.009		0.777±0.009		0.797±0.005		0.635±0.008	
	k=200	0.750±0.005	1.08	0.609±0.006	1.50	0.783±0.006	0.77	0.800 ± 0.002	0.38	0.642±0.005	1.10
	k=400	0.761±0.006	2.56	0.619±0.007	3.17	0.790±0.004	1.67	0.798±0.002	0.13	0.646±0.002	1.73
	k=600	0.764 ± 0.005	2.96	0.624 ± 0.007	4.00	0.797 ± 0.003	2.57	0.799±0.002	0.25	0.653 ± 0.004	2.83
	k=800	0.760±0.004	2.43	0.618±0.007	3.00	0.794±0.005	2.19	0.798±0.002	0.13	0.649±0.006	2.20

Table 16: Effect of Augmented Macrophages for Nuclei Segmentation on MoNuSAC

Model	Augmentation	DICE	↑ (%)	AJI	↑ (%)	DQ	↑ (%)	SQ	↑ (%)	PQ	↑ (%)
SONNET	Baseline	0.774±0.006		0.624±0.006		0.788±0.007		0.797±0.003		0.643±0.004	
	k=200	0.779±0.003	0.65	0.631±0.003	1.12	0.795 ± 0.003	0.89	0.811±0.010	1.76	0.650 ± 0.003	1.09
	k=400	0.780±0.002	0.78	0.633 ± 0.003	1.44	0.792±0.007	0.51	0.804±0.006	0.88	0.648±0.004	0.78
	k=600	0.782 ± 0.001	1.03	0.630±0.004	0.96	0.795±0.005	0.89	0.816 ± 0.003	2.38	0.650±0.004	1.09
	k=800	0.776±0.002	0.26	0.625±0.005	0.16	0.787±0.003	-0.13	0.802±0.006	0.63	0.643±0.000	0.00
PointNu	Baseline	0.742±0.010		0.600±0.009		0.777±0.009		0.797±0.005		0.635±0.008	
	k=200	0.752±0.004	1.35	0.609±0.006	1.50	0.789±0.010	1.54	0.797±0.003	0.00	0.644±0.006	1.42
	k=400	0.766 ± 0.004	3.23	0.624 ± 0.005	4.00	0.799 ± 0.002	2.83	0.800 ± 0.000	0.38	0.655 ± 0.002	3.15
	k=600	0.756±0.004	1.89	0.614±0.004	2.33	0.790±0.004	1.67	0.799±0.004	0.25	0.647±0.002	1.89
	k=800	0.754±0.007	1.62	0.611±0.007	1.83	0.782±0.007	0.64	0.800 ± 0.000	0.38	0.641±0.006	0.94

Table 17: Effect of Augmented Macrophages and Neutrophils for Nuclei Segmentation on MoNuSAC

Model	Augmentation	DICE	↑ (%)	AJI	↑ (%)	DQ	↑ (%)	SQ	↑ (%)	PQ	↑ (%)
SONNET	Baseline	0.774±0.006		0.624±0.006		0.788±0.007		0.797±0.003		0.643±0.004	
	k=200	0.775±0.003	-0.13	0.628±0.002	0.64	0.795 ± 0.0032	0.89	0.812 ± 0.011	1.88	0.652 ± 0.004	1.40
	k=400	0.777±0.003	0.39	0.628±0.007	0.64	0.788±0.003	0.00	0.803±0.004	0.75	0.644±0.003	0.16
	k=600	0.781 ± 0.005	0.90	0.632 ± 0.007	1.28	0.794±0.008	0.76	0.809±0.006	1.51	0.649±0.004	0.93
	k=800	0.775±0.003	0.13	0.626±0.004	0.32	0.794±0.004	0.76	0.811±0.011	1.76	0.649±0.003	0.93
PointNu	Baseline	0.742±0.010		0.600±0.009		0.777±0.009		0.797±0.005		0.635±0.008	
	k=200	0.758 ± 0.002	2.16	0.614±0.000	2.33	0.787±0.003	1.29	0.800 ± 0.002	0.38	0.646±0.001	1.73
	k=400	0.758±0.010	2.16	0.612±0.013	2.00	0.788±0.013	1.42	0.798±0.003	0.13	0.645±0.012	1.57
	k=600	0.757±0.000	2.02	0.616 ± 0.002	2.67	0.795 ± 0.002	2.32	0.796±0.000	-0.13	0.649 ± 0.002	2.20
	k=800	0.749±0.004	0.94	0.603±0.005	0.50	0.787±0.002	1.29	0.793±0.005	-0.50	0.640±0.003	0.79

Table 18: Effect of Augmented Miscellaneous Nuclei for Nuclei Classification on CoNSEP

Model	Augmentation	F_d	\uparrow (%)	Acc	\uparrow (%)	F_c^M	\uparrow (%)	F_c^I	\uparrow (%)	F_c^E	\uparrow (%)	F_c^S	\uparrow (%)
SONNET	Baseline	0.741±0.003		0.852±0.003		0.352±0.051		0.595±0.006		0.607±0.010		0.555±0.008	
	k=200	0.733±0.002	-1.08	0.854±0.002	0.23	0.378±0.014	7.39	0.603 ± 0.006	1.34	0.601±0.006	-0.99	0.547±0.005	-1.44
	k=400	0.745 ± 0.005	0.54	0.854±0.005	0.23	0.422 ± 0.018	19.89	0.602±0.018	1.18	0.618 ± 0.012	1.81	0.547±0.007	-1.44
	k=600	0.742±0.002	0.13	0.855 ± 0.002	0.35	0.410±0.041	16.48	0.598±0.016	0.50	0.608±0.004	0.16	0.555 ± 0.005	0.00
	k=800	0.725±0.003	-2.16	0.851±0.003	-0.12	0.383±0.025	8.81	0.598±0.014	0.50	0.580±0.007	-4.45	0.544±0.006	-1.98
PointNu	Baseline	0.724±0.003		0.888±0.005		0.544±0.021		0.661±0.020		0.620±0.014		0.542±0.014	
	k=200	0.741±0.007	2.35	0.892±0.001	0.45	0.576±0.008	5.88	0.670±0.006	1.36	0.646±0.009	4.19	0.554±0.003	2.21
	k=400	0.751 ± 0.004	3.73	0.892±0.003	0.45	0.585±0.012	7.54	0.669±0.010	1.21	0.657 ± 0.007	5.97	0.561±0.007	3.51
	k=600	0.744±0.004	2.76	0.897 ± 0.007	1.01	0.600 ± 0.005	10.29	0.680 ± 0.006	2.87	0.651±0.009	5.00	0.558±0.019	2.95
	k=800	0.744±0.005	2.76	0.892±0.002	0.45	0.578±0.004	6.25	0.664±0.011	0.45	0.646±0.011	4.19	0.562 ± 0.002	3.69

Table 19: Effect of Augmented Miscellaneous Nuclei for Nuclei Classification on GLySAC

Model	Augmentation	F_d	\uparrow (%)	Acc	\uparrow (%)	F_c^M	\uparrow (%)	F_c^L	\uparrow (%)	F_c^E	\uparrow (%)
SONNET	Baseline	0.838±0.003		0.698±0.004		0.287±0.05		0.520±0.007		0.540±0.005	
	k=200	0.839±0.005	0.12	0.707 ± 0.002	1.29	0.305±0.005	6.27	0.529±0.002	1.73	0.545±0.007	0.93
	k=400	0.844 ± 0.004	0.72	0.704±0.002	0.86	0.309±0.008	7.67	0.523±0.011	0.58	0.549 ± 0.011	1.67
	k=600	0.843±0.004	0.60	0.706±0.005	1.15	0.310 ± 0.011	8.01	0.531 ± 0.013	2.12	0.545±0.003	0.93
	k=800	0.840±0.005	0.24	0.702±0.003	0.57	0.301±0.009	4.88	0.520±0.007	0.00	0.545±0.002	0.93
PointNu	Baseline	0.824±0.002		0.715±0.010		0.294±0.010		0.518±0.019		0.553±0.004	
	k=200	0.833±0.005	1.09	0.724±0.010	1.26	0.307±0.011	4.42	0.536±0.021	3.47	0.566±0.007	2.35
	k=400	0.832±0.004	0.97	0.720±0.006	0.70	0.314±0.006	6.80	0.529±0.008	2.12	0.561±0.008	1.45
	k=600	0.832±0.005	0.97	0.720±0.006	0.70	0.318 ± 0.004	8.16	0.525±0.005	1.35	0.563±0.010	1.81
	k=800	0.835 ± 0.005	1.33	0.725 ± 0.004	1.40	0.309±0.005	5.10	0.536 ± 0.007	3.47	0.571 ± 0.005	3.25

Table 20: Effect of Augmented Neutrophils for Nuclei Classification on MoNuSAC

Model	Augmentation	F_d	\uparrow (%)	Acc	\uparrow (%)	F_c^E	\uparrow (%)	F_c^L	\uparrow (%)	F_c^M	\uparrow (%)	F_c^N	\uparrow (%)
SONNET	Baseline	0.830±0.001		0.939±0.004		0.709±0.005		0.786±0.008		0.511±0.017		0.514±0.028	
	k=200	0.832±0.004	0.20	0.957 ± 0.001	1.92	0.741 ± 0.007	4.51	0.811 ± 0.006	3.18	0.542 ± 0.006	6.07	0.532 ± 0.005	3.50
	k=400	0.832±0.003	0.24	0.950±0.004	1.17	0.740±0.013	4.37	0.799±0.018	1.65	0.529±0.012	3.52	0.517±0.007	-0.78
	k=600	0.827±0.003	-0.36	0.946±0.004	0.75	0.725±0.002	2.26	0.787±0.016	0.13	0.529±0.004	3.52	0.503±0.005	-2.14
	k=800	0.832 ± 0.001	0.24	0.943±0.005	0.43	0.721±0.006	1.69	0.794±0.014	1.02	0.514±0.007	0.59	0.525±0.006	2.14
PointNu	Baseline	0.835±0.001		0.975±0.001		0.786±0.004		0.828±0.007		0.501±0.018		0.508±0.036	
	k=200	0.838±0.005	0.36	0.978 ± 0.000	0.31	0.795 ± 0.007	1.15	0.832±0.009	0.48	0.537±0.027	7.19	0.550 ± 0.019	8.27
	k=400	0.839±0.005	0.48	0.976±0.000	0.10	0.788±0.004	0.25	0.832±0.007	0.48	0.552±0.035	10.18	0.528±0.003	3.94
	k=600	0.839±0.005	0.48	0.976±0.000	0.10	0.794±0.008	1.02	0.829±0.002	0.12	0.534±0.011	6.59	0.538±0.021	5.91
	k=800	0.840 ± 0.004	0.60	0.975±0.001	0.00	0.790±0.007	0.51	0.832 ± 0.004	0.48	0.557 ± 0.014	11.18	0.515±0.008	1.38

Table 21: Effect of Augmented Macrophages for Nuclei Classification on MoNuSAC

Model	Augmentation	F_d	\uparrow (%)	Acc	\uparrow (%)	F_c^E	\uparrow (%)	F_c^L	\uparrow (%)	F_c^M	\uparrow (%)	F_c^N	\uparrow (%)
SONNET	Baseline	0.830±0.001		0.939±0.004		0.709±0.005		0.786±0.008		0.511±0.017		0.514±0.028	
	k=200	0.832±0.008	0.24	0.940±0.008	0.11	0.719±0.006	1.41	0.787±0.010	0.13	0.536±0.013	4.89	0.526±0.033	2.23
	k=400	0.836 ± 0.004	0.72	0.948±0.003	0.96	0.736±0.004	3.81	0.798±0.007	1.53	0.565 ± 0.011	10.57	0.544 ± 0.029	5.84
	k=600	0.835±0.002	0.60	0.952 ± 0.007	1.38	0.746 ± 0.010	5.22	0.801 ± 0.006	1.92	0.532±0.009	4.11	0.535±0.019	4.09
	k=800	0.829±0.006	-0.12	0.950±0.007	1.17	0.738±0.016	4.09	0.793±0.014	0.89	0.536±0.004	4.89	0.539±0.018	4.86
PointNu	Baseline	0.835±0.001		0.975±0.001		0.786±0.004		0.828±0.007		0.501±0.018		0.508±0.036	
	k=200	0.838±0.006	0.36	0.977 ± 0.002	0.21	0.793±0.002	0.89	0.832±0.009	0.48	0.535±0.018	6.79	0.511±0.014	0.59
	k=400	0.839±0.004	0.48	0.976±0.000	0.10	0.793±0.006	0.89	0.832±0.002	0.48	0.542±0.018	8.18	0.524±0.018	3.15
	k=600	0.840±0.006	0.60	0.976±0.001	0.10	0.796 ± 0.006	1.27	0.832±0.003	0.48	0.545 ± 0.003	8.78	0.528 ± 0.008	3.94
	k=800	0.840 ± 0.002	0.60	0.976±0.003	0.10	0.794±0.006	1.02	0.833 ± 0.001	0.60	0.524±0.018	4.59	0.509±0.017	0.20

Table 22: Effect of Augmented Macrophages and Neutrophils for Nuclei Classification on MoNuSAC

Model	Augmentation	F_d	\uparrow (%)	Acc	\uparrow (%)	F_c^E	\uparrow (%)	F_c^L	\uparrow (%)	F_c^M	\uparrow (%)	F_c^N	\uparrow (%)
SONNET	Baseline	0.830±0.001		0.939±0.004		0.709±0.005		0.786±0.008		0.511±0.017		0.514±0.028	
	k=200	0.834 ± 0.003	0.48	0.943±0.002	0.43	0.731±0.006	3.10	0.788±0.004	0.25	0.541±0.021	5.87	0.520±0.014	1.17
	k=400	0.829±0.003	-0.12	0.941±0.007	0.21	0.721±0.014	1.69	0.785±0.009	-0.13	0.524±0.010	2.54	0.518±0.020	0.78
	k=600	0.830±0.001	0.00	0.954 ± 0.003	1.60	0.740 ± 0.018	4.37	0.802 ± 0.007	2.04	0.548 ± 0.014	7.24	0.538 ± 0.006	4.67
	k=800	0.831±0.003	0.12	0.946±0.005	0.75	0.736±0.003	3.81	0.790±0.011	0.51	0.501±0.027	-1.96	0.518±0.016	0.78
PointNu	Baseline	0.835±0.001		0.975±0.001		0.786±0.004		0.828±0.007		0.501±0.018		0.508±0.036	
	k=200	0.842±0.002	0.84	0.976 ± 0.001	0.10	0.797±0.001	1.40	0.835 ± 0.002	0.85	0.524±0.013	4.59	0.524±0.009	3.15
	k=400	0.839±0.004	0.48	0.975±0.001	0.00	0.794±0.008	1.02	0.830±0.002	0.24	0.534±0.013	6.59	0.526±0.015	3.54
	k=600	0.844 ± 0.002	1.08	0.974±0.003	-0.10	0.799 ± 0.008	1.65	0.829±0.007	0.12	0.534 ± 0.018	6.59	0.530 ± 0.013	4.33
	k=800	0.839±0.005	0.48	0.972±0.004	-0.31	0.789±0.012	0.38	0.824±0.011	-0.48	0.518±0.008	3.39	0.518±0.016	1.97

rare-type nuclei. It requires the major-type nucleus to be larger, allowing the rare-type nucleus to be placed within its region, and the neighboring pixels of the rare-type nucleus are updated using a weighted sum of their original surroundings. While these methods can integrate the existing rare-type nuclei into new environments, none of them analyzes or leverages the relationship between the original neighboring environments of rare-type nuclei and the new environments into which where they are inserted. In contrast, NucleiMix improves upon these methods by adopting a context-aware probabilistic sampling strategy, which probabilistically selects appropriate positions for augmenting rare-type nuclei, under the assumption that the more similar environments between the original and target positions, the more realistic the augmentation will be.

Diffusion Models have achieved unprecedented success in solving inverse problems, and we leverage this capability to mitigate artifacts introduced by data augmentations in nuclei instance segmentation. Diffusion models can be adopted to generate new instances of nuclei as a sufficient number of instances are provided. When it comes to rare-type nuclei, it becomes impossible to reliably train any model to produce realistic nuclei. Pre-trained diffusion models can also be used for direct inpainting of surrounding regions as mixing existing nuclei with new environments; however, this often results in obscure boundaries and inconsistent surroundings. To address this, NucleiMix introduces a progressive inpainting strategy that imposes spatial restrictions on the inpainted areas, ensuring that the newly generated environments are coherent while maintaining sharp, well-defined boundaries for rare-type nuclei (Fig. 3). This approach, however, comes at the cost of increased computational complexity per instance. Further investigation is needed to expedite the inpainting process and reduce computational costs.

NucleiMix demonstrated improvements in both segmentation and classification performance for various types of nuclei in three public datasets. However, other augmentation methods often resulted in worse performance than the baseline where no synthesized nuclei were added and used. The improved performance obtained by NucleiMix may be ascribable to its context-aware probabilistic sampling for candidate location selection and progressive inpainting for realistic reconstruction of new environments. The former ensures that rare-type nuclei are placed in similar environments, and the latter seamlessly integrates the rare-type nuclei into their new environment. In contrast, other augmentation methods tend to produce unrealistic or awkward nuclei, which could adversarially affect the performance of nuclei instance

segmentation. Moreover, NucleiMix generally improved the nuclei instance segmentation performance with varying numbers of augmented rare-type nuclei. Overall, $k=600$ was found to be the optimal number of augmented nuclei. The smaller numbers of augmented nuclei (e.g., $k=200$) resulted in fewer improvements, and adding more augmented nuclei (e.g., $k=800$) did not consistently lead to better performance. This suggests that the performance tends to saturate after a certain number of augmented nuclei is introduced.

This study has several limitations. First, we adopted GMM to learn the distribution of rare-type nuclei in the feature space and to predict the likelihood of major-type and background locations. Although the nuclei instance segmentation performance was improved, the accuracy of the predicted candidate locations cannot be fully guaranteed and may vary on a case-by-case basis. Second, the use of a diffusion model for inpainting introduces stochasticity and leads to time-consuming reconstructions, which are its inherent limitations. Future work will focus on leveraging advanced samplers designed to accelerate the inference speed of the diffusion model. Third, NucleiMix affects the nuclei instance segmentation performance not only for rare-type nuclei but also for major-type nuclei. This may be attributed to the Copy-Replace operation applied to major-type nuclei, which reduces their overall number. The relationship between the major-type and rare-type nuclei with respect to nuclei instance segmentation, as well as the impact of the Copy-Replace operation, needs further investigation. Fourth, the performance gains obtained by NucleiMix tended to plateau after reaching a specific number of augmented nuclei. This may be due to the limited availability of rare-type nuclei. Although NucleiMix introduces new environments, its effectiveness is ultimately constrained by the number of available rare-type nuclei for augmentation. Last, three public datasets and two backbone models were utilized in this study. To further confirm the effectiveness of NucleiMix, an extended validation study including additional datasets and backbone models should be followed.

7. Conclusion

Herein, we propose NucleiMix, a data augmentation method designed to improve the performance and robustness of nuclei segmentation and classification tasks. NucleiMix analyzes the environments of various nuclei types to identify suitable positions for augmenting rare-type nuclei. Then, it employs a progressive inpainting strategy with a diffusion model to complete

the generation of realistic, synthetic rare-type nuclei. The results show that NucleiMix can generate natural-looking augmented nuclei, leading to improved performance of nuclei segmentation and classification. The superior performance on three public datasets (CoNSeP, GLySAC, and MoNuSAC) with two backbone models (SONNET and PointNu) highlights the ability of NucleiMix to address data scarcity and imbalance in nuclei instance segmentation. In a follow-up study, we will further investigate the application of NucleiMix to other types of nuclei and tissue components to augment tissue images more broadly.

Acknowledgments

This study was supported by a grant of the National Research Foundation of Korea (NRF) (No. 2021R1A2C2014557 and No. RS-2024-00397293) and by the Ministry of Trade, Industry and Energy(MOTIE) and Korea Institute for Advancement of Technology (KIAT) through the International Cooperative R&D program (P0022543).

References

- Anderson, D.O., B., 1982. "reverse-time diffusion equation models". *Stochastic Processes and their Applications* 12.3, 313–326.
- Barocas, A., D., et al., 2007. "renal cell carcinoma sub-typing by histopathology and fluorescence in situ hybridization on a needle-biopsy specimen". *BJU international* 99.2, 290–295.
- Burke, B., H., et al., 1997. "artificial neural networks improve the accuracy of cancer survival prediction". *Cancer* 79.4, 857–862.
- Chung, Hyungjin, et al., 2022a. "diffusion posterior sampling for general noisy inverse problems", in: *arXiv preprint arXiv:2209.14687*.
- Chung, Hyungjin, et al., 2022b. "improving diffusion models for inverse problems using manifold constraints", in: *Advances in Neural Information Processing Systems*, pp. 25683–25696.
- Cossio, M., 2023. "augmenting medical imaging: a comprehensive catalogue of 65 techniques for enhanced data analysis", in: *arXiv preprint arXiv:2303.01178*.

- DeVries, Terrance, , Taylor., G.W., 2017. "improved regularization of convolutional neural networks with cutout", in: arXiv preprint arXiv:1708.04552.
- Dhariwal, Prafulla, , Nichol., A., 2021. "diffusion models beat gans on image synthesis", in: Advances in neural information processing systems 34, pp. 8780–8794.
- Doan, Nhat, T.N., et al., 2022a. "gradmix for nuclei segmentation and classification in imbalanced pathology image datasets", in: International Conference on Medical Image Computing and Computer-Assisted Intervention. Cham: Springer Nature Switzerland, pp. 171–180.
- Doan, NN, T., et al., 2022b. "sonnet: A self-guided ordinal regression neural network for segmentation and classification of nuclei in large-scale multi-tissue histology images". IEEE Journal of Biomedical and Health Informatics 26, 3218–3228.
- Ebrahimi, A., M., , Lunasin., E., 2013. "the navier–stokes–voight model for image inpainting". The IMA Journal of Applied Mathematics 78.5, 869–894.
- Efron, Bradley., 2011. "tweedie’s formula and selection bias". Journal of the American Statistical Association 106.496, 1602–1614.
- Feng, Ruiwei, et al., 2020. "a deep learning approach for colonoscopy pathology wsi analysis: accurate segmentation and classification". IEEE Journal of Biomedical and Health Informatics 25(10), 3700–3708.
- Gamper, Jevgenij, et al., 2019. "pannuke: an open pan-cancer histology dataset for nuclei instance segmentation and classification". Digital Pathology: 15th European Congress, ECDP 2019, Warwick, UK, April 10–13, 2019, Proceedings 15, 10–13.
- Ghiasi, Golnaz, et al., 2021. "simple copy-paste is a strong data augmentation method for instance segmentation", in: Proceedings of the IEEE/CVF conference on computer vision and pattern recognition, pp. 2918–2928.
- Goodfellow, Ian, et al., 2022. "generative adversarial networks". Communications of the ACM 63, 139–144.

- Graham, Simon, et al., 2019. "hover-net: Simultaneous segmentation and classification of nuclei in multi-tissue histology images". *Medical image analysis* 58, 101563.
- He, Lei, et al., 2012. "histology image analysis for carcinoma detection and grading". *Computer methods and programs in biomedicine* 107.3, 538–556.
- Ho, Jonathan, Jain, A., , Abbeel, P., 2020. "denoising diffusion probabilistic models", in: *Advances in neural information processing systems*, pp. 6840–6851.
- Hollandi, Reka, et al., 2022. "nucleus segmentation: towards automated solutions.". *Trends in Cell Biology* 32.4, 295–310.
- Hussain, Zeshan, et al., 2017. "differential data augmentation techniques for medical imaging classification tasks". *AMIA annual symposium proceedings 2017*, 979.
- Kirillov, Alexander, et al., 2019. "panoptic segmentation.", in: *Proceedings of the IEEE/CVF conference on computer vision and pattern recognition.*, pp. 9404–9413.
- Kumar, Neeraj, et al., 2017a. "a dataset and a technique for generalized nuclear segmentation for computational pathology.". *IEEE transactions on medical imaging* 36.7, 1550–1560.
- Kumar, Neeraj, et al., 2017b. "a dataset and a technique for generalized nuclear segmentation for computational pathology.". *IEEE transactions on medical imaging* 36.7, 1550–1560.
- Lugmayr, Andreas, et al., 2022. "repaint: Inpainting using denoising diffusion probabilistic models." 2022., in: *Proceedings of the IEEE/CVF conference on computer vision and pattern recognition.*, pp. 11461–11471.
- Naglah, Ahmed, et al., 2022. "conditional gans based system for fibrosis detection and quantification in hematoxylin and eosin whole slide images". *Medical image analysis* 81, 102537.
- Nunes, D., J., et al., 2024. "a survey on cell nuclei instance segmentation and classification: Leveraging context and attention.". *arXiv preprint arXiv:2407.18673*. URL: <https://arxiv.org/abs/2407.18673>.

- Reynolds, A., D., 2009. "gaussian mixture models", in: Encyclopedia of biometrics, pp. 741.659–663.
- van Rijsbergen, Joost, C., 1979. Information retrieval. Butterworth-Heinemann.
- Sirazitdinov, Ilyas, et al., 2019. "data augmentation for chest pathologies classification". 2019 IEEE 16th international symposium on biomedical imaging 2019, 1216–1219.
- Sohl-Dickstein, Jascha, et al., 2015. "deep unsupervised learning using nonequilibrium thermodynamics", in: International conference on machine learning, pp. 2256–2265.
- Song, Jiaming, Meng, C., , Ermon., S., 2020a. "denoising diffusion implicit models.", in: arXiv preprint arXiv:2010.02502.
- Song, Yang, et al., 2020b. "score-based generative modeling through stochastic differential equations", in: arXiv preprint arXiv:2011.13456.
- Takahashi, Ryo, Matsubara, T., Uehara., K., 2019. "data augmentation using random image cropping and patching for deep cnns". IEEE Transactions on Circuits and Systems for Video Technology 30.9, 2917–2931.
- Tellez, David, et al., 2019. "quantifying the effects of data augmentation and stain color normalization in convolutional neural networks for computational pathology". Medical image analysis 58, 101544.
- Verma, Ruchika, et al., 2021. "monusac2020: A multi-organ nuclei segmentation and classification challenge". IEEE Transactions on Medical Imaging 40, 3413–3423.
- Vu, et al., Q.D., 2019. "methods for segmentation and classification of digital microscopy tissue images.". Frontiers in bioengineering and biotechnology 7, 433738.
- Wang, Xiyue, et al., 2022. "transformer-based unsupervised contrastive learning for histopathological image classification". IEEE Trans. Vis. Comput. Graph. 81, 102559.

- Yao, Kai, et al., 2023. "pointnu-net: Keypoint-assisted convolutional neural network for simultaneous multi-tissue histology nuclei segmentation and classification". *IEEE Transactions on Emerging Topics in Computational Intelligence* 8(a), 802–813.
- Yun, Sangdoon, et al., 2019. "cutmix: Regularization strategy to train strong classifiers with localizable features", in: *Proceedings of the IEEE/CVF international conference on computer vision*, p. 1708.04552.
- Zhang, Hongyi, et al., 2017. "mixup: Beyond empirical risk minimization", in: *arXiv preprint arXiv:1710.09412*.